

1 A set of molecular models based on quantum
2 mechanical *ab initio* calculations and
3 thermodynamic data

4 Bernhard Eckl, Jadran Vrabec*, and Hans Hasse

5 Institut für Technische Thermodynamik und Thermische
6 Verfahrenstechnik, Universität Stuttgart
7 Pfaffenwaldring 9, 70550 Stuttgart, Germany

8 **Abstract**

9 A parameterization strategy for molecular models on the basis of force
10 fields is proposed, which allows a rapid development of models for small
11 molecules by using results from quantum mechanical (QM) *ab initio* calcu-
12 lations and thermodynamic data. The geometry of the molecular models
13 is specified according to the atom positions determined by QM energy
14 minimization. The electrostatic interactions are modeled by reducing the
15 electron density distribution to point dipoles and point quadrupoles lo-
16 cated in the center of mass of the molecules. Dispersive and repulsive
17 interactions are described by Lennard-Jones sites, for which the param-
18 eters are iteratively optimized to experimental vapor-liquid equilibrium
19 (VLE) data, i.e. vapor pressure, saturated liquid density, and enthalpy of
20 vaporization of the considered substance. The proposed modeling strat-
21 egy was applied to a sample set of ten molecules from different substance
22 classes. New molecular models are presented for iso-butane, cyclohexane,

*Tel.: +49-711/685-66107, Fax: +49-711/685-66140, Email: vrabec@itt.uni-stuttgart.de

23 formaldehyde, dimethyl ether, sulfur dioxide, dimethyl sulfide, thiophene,
24 hydrogen cyanide, acetonitrile, and nitromethane. Most of the models
25 are able to describe the experimental VLE data with deviations of a few
26 percent.

27 **Keywords:** Molecular modeling; modeling strategy; vapor-liquid equilibrium;
28 critical properties; iso-butane; cyclohexane; formaldehyde; dimethyl ether; sul-
29 fur dioxide; dimethyl sulfide; thiophene; hydrogen cyanide; acetonitrile; ni-
30 tromethane

1 Introduction

32 Molecular modeling and simulation is a progressive approach for describing
33 and predicting thermophysical properties of both pure substances and mixtures
34 of technical interest. Many authors have shown the excellent capabilities of
35 this molecular approach for different applications [1, 2]. Unfortunately, the
36 more widespread use of molecular methods for engineering applications is still
37 restricted by the scarcity of suitable molecular models.

38 For many substances, transferable molecular models have been developed,
39 i.e. force fields for classes of compounds like alkanes or alcohols. Thereby,
40 it is assumed that the parameters for functional groups are valid for different
41 molecular species. The main disadvantage of transferable models is that their
42 parameters were adjusted for the whole substance class and may not be optimal
43 for a specific substance. Furthermore, they do not cover substances outside the
44 modeled class. An overview and assessment of some commonly used transferable
45 potentials can be found in [3].

46 Molecular models that were optimized for specific substances are available
47 only for selected compounds and, particularly older ones, sometimes do not show
48 the desired quality. Therefore, from an engineering point of view, a method for
49 the rapid development of new molecular models for specific substances is of
50 great interest. Moreover, the molecular models should be accurate, simple,

51 and computationally efficient. In the present paper, a systematic strategy is
52 proposed to develop such models.

53 The present work is restricted to rigid, non-polarizable models for com-
54 paratively small molecules. The models have state-independent parameters
55 throughout. For computational efficiency, the united-atom approach is used,
56 i.e. hydrogen atoms bonded to carbon are not modeled explicitly. The proposed
57 strategy uses information determined by quantum mechanical (QM) *ab initio*
58 calculations to include physically sound molecular properties and to reduce the
59 number of adjustable parameters. A remaining subset of model parameters –
60 typically two to four – is subsequently optimized by adjustment to experimen-
61 tal data on vapor-liquid equilibria (VLE) of the pure substances. The aim is
62 to achieve deviations to experimental values for the vapor pressure, saturated
63 liquid density, and enthalpy of vaporization in the range from triple point to
64 critical point of below 5, 1, and 5%, respectively.

65 Such accurate models are known to have an excellent extrapolative and pre-
66 dictive power. This was recently shown, e.g., by the prediction of 17 different
67 thermophysical properties for ethylene oxide, covering phase equilibria, thermal,
68 caloric, transport properties, and surface tension [4], or for ammonia including
69 structural quantities [5].

70 Molecular models that were developed on the basis of QM calculations stand
71 between strictly *ab initio* models and fully empirical models. The present strat-
72 egy is based on the idea to include substantial *ab initio* information without giv-
73 ing up the freedom to reasonably optimize the model to important macroscopic
74 thermodynamic properties. Thus, for the modeling process some experimental
75 data is needed for optimization. All three chosen properties, mentioned above,
76 have the advantage to be well available for numerous engineering fluids and to
77 represent dominant features of the fluid state.

78 The parameters of a molecular model can be separated into three groups.
79 Firstly, geometric parameters specify the locations of the different interaction
80 sites of the molecular model. Secondly, electrostatic parameters define the in-

81 teractions of static polarities of the single molecules. And finally, dispersive
 82 and repulsive parameters determine the attraction by London forces and the
 83 repulsion by overlaps of the electronic orbitals. Here, the Lennard-Jones 12-6
 84 (LJ) potential [6, 7] was used to assure straightforward compatibility with the
 85 overwhelming majority of the molecular models in the literature.

86 To describe the intermolecular interactions, a varying number of LJ sites
 87 and superimposed ideal point dipoles and/or ideal linear point quadrupoles
 88 were used. Point dipoles or quadrupoles were employed for the description of
 89 the electrostatic interactions to reduce the computational effort significantly.
 90 A point dipole may, e.g. when a simulation program does not support this
 91 interaction site type, be approximated by two point charges $\pm q$ separated by
 92 a distance l . Limited to small l , one is free to choose this distance as long as
 93 $\mu = ql$ holds. Analogously, a point quadrupole can be approximated by three
 94 collinear point charges q , $-2q$, and q separated by l each, where $Q = 2ql^2$.

95 The total intermolecular interaction energy writes as

$$\begin{aligned}
 U = & \sum_{i=1}^{N-1} \sum_{j=i+1}^N \left\{ \sum_{a=1}^{S_i^{LJ}} \sum_{b=1}^{S_j^{LJ}} 4\epsilon_{ijab} \left[\left(\frac{\sigma_{ijab}}{r_{ijab}} \right)^{12} - \left(\frac{\sigma_{ijab}}{r_{ijab}} \right)^6 \right] + \right. \\
 & \left. \sum_{c=1}^{S_i^e} \sum_{d=1}^{S_j^e} \frac{1}{4\pi\epsilon_0} \left[\frac{\mu_{ic}\mu_{jd}}{r_{ijcd}^3} \cdot f_1(\boldsymbol{\omega}_i, \boldsymbol{\omega}_j) + \frac{\mu_{ic}Q_{jd} + Q_{ic}\mu_{jd}}{r_{ijcd}^4} \cdot f_2(\boldsymbol{\omega}_i, \boldsymbol{\omega}_j) + \frac{Q_{ic}Q_{jd}}{r_{ijcd}^5} \cdot f_3(\boldsymbol{\omega}_i, \boldsymbol{\omega}_j) \right] \right\}, \tag{1}
 \end{aligned}$$

96 where r_{ijab} , ϵ_{ijab} , σ_{ijab} are the distance, the LJ energy parameter, and the
 97 LJ size parameter, respectively, for the pair-wise interaction between LJ site a
 98 on molecule i and LJ site b on molecule j . ϵ_0 is the permittivity of vacuum,
 99 whereas μ_{ic} and Q_{ic} denote the dipole moment and the quadrupole moment of
 100 the electrostatic interaction site c on molecule i , and so forth. $f_x(\boldsymbol{\omega}_i, \boldsymbol{\omega}_j)$ are
 101 expressions for the dependency of the electrostatic interactions on the orienta-
 102 tions $\boldsymbol{\omega}_i$ and $\boldsymbol{\omega}_j$ of the molecules i and j , cf. [8, 9]. Finally, the summation
 103 limits N , S_x^{LJ} , and S_x^e denote the number of molecules, the number of LJ sites,
 104 and the number of electrostatic sites, respectively.

105 Interactions between LJ sites of different type are determined by applying
106 the standard Lorentz-Berthelot combining rules [10, 11]

$$\sigma_{ijab} = \frac{\sigma_{iaaa} + \sigma_{jjbb}}{2}, \quad (2)$$

108 and

$$\varepsilon_{ijab} = \sqrt{\varepsilon_{iaaa}\varepsilon_{jjbb}}. \quad (3)$$

12 Molecular properties from QM

111 In a recent publication, Sandler et al. [12] gives a brief overview on the
112 use of QM for the calculation of thermophysical properties. By numerically
113 solving Schrödinger’s equation, it is nowadays possible to calculate different
114 molecular properties for technically relevant components in a quite standardized
115 way. Many different QM codes are available for this task. For license reasons,
116 the open source code GAMESS(US) [13] was used in the present work.

12.1 Geometry

118 All geometric data of the molecular models, i.e. bond lengths, angles, and
119 dihedrals, were directly taken from QM calculations. Therefore, a geome-
120 try optimization, i.e. an energy minimization, was initially performed using
121 GAMESS(US) [13]. The Hartree-Fock level of theory was applied with a rela-
122 tively small (6-31G) basis set. Alternatively, density functional theory (DFT)
123 methods, e.g. BLY3P, can be used, as they are known to give reasonable results
124 for the molecular structure [14].

125 The resulting configuration of the atoms was taken without subsequent mod-
126 ification to specify the position of the LJ sites in space, except for the hydrogen
127 atoms. As the united atom approach was used to obtain computationally ef-
128 ficient molecular models, the hydrogen atoms were modeled together with the
129 carbon atom they are bonded to. For the methylene (CH_2) and methyl (CH_3)
130 united atom sites, the LJ potential was located at the geometric mean of the
131 nuclei, while the methine (CH) united atom site was located at 0.4 of the dis-

132 tance between carbon and hydrogen atom, cf. Figure 1. These empirical offsets
133 are in good agreement with the results of Ungerer et al. [15], which were found
134 by optimization of transferable molecular models for n-alkanes.

132.2 Electrostatics

136 Intermolecular electrostatic interactions mainly occur due to static polarities
137 of single molecules that can well be obtained by QM. Here, the Møller-Plesset
138 2 level was used that considers electron correlation in combination with the
139 polarizable 6-311G(d,p) basis set.

140 The purpose of the present work is the development of effective pair poten-
141 tials with a state-independent set of model parameters. Obviously, the electro-
142 static interactions are stronger in the liquid state than in the gaseous state due
143 to the higher density. Furthermore, the mutual polarization raises their mag-
144 nitude in the liquid. Thus, for the calculation of the electrostatic moments by
145 QM a liquid-like state should be considered. This was done here by placing the
146 molecule within a dielectric continuum and assigning the experimental dielectric
147 constant of the liquid to it, as in the COSMO method [16].

148 From the resulting electron density distribution for the small symmetric
149 molecules regarded here, ideal point dipoles and ideal linear point quadrupoles
150 were estimated by simple integration over the orbitals. Magnitudes and orien-
151 tations of these electrostatic interaction sites were used in the molecular models
152 without any modification.

153 For other, more complex molecules, more sophisticated methods like CHELP
154 [17], CHELPG [18], or the distributed multipole analysis [19] are available in
155 the literature. These methods adjust a set of partial charges or higher order
156 electrostatic sites to the electrostatic potential around the molecule calculated
157 by QM. Although they are able to reflect the electrostatic interactions with
158 higher accuracy, they are not considered here. They always yield a larger number
159 of interaction sites if they are not co-located with other sites and would thus
160 lead to computationally more expensive molecular models.

2.3 Dispersion and Repulsion

162 It would be highly desirable to also calculate the dispersive and repulsive
163 interactions using *ab initio* methods as well. This approach was followed by
164 different authors in the past, e.g. for neon [20, 21, 22, 23], argon [21, 23, 24],
165 krypton [25], nitrogen [26], carbon dioxide [27], hydrogen chloride [28], acetoni-
166 trile [29], methanol [29], acetylene [30], and methanethiol [31]. However, from
167 an engineering point of view, this leads to difficulties.

168 For an estimation of dispersive and repulsive interactions at least two molecules
169 must be taken into account. To properly scan the energy hyper surface, many
170 QM calculations at different distances and orientations of the molecules have to
171 be performed. As the dispersive, and partly also the repulsive, interactions are
172 just a very small fraction of the total energy calculated by QM, highly accurate
173 methods like coupled cluster (CC) with large basis sets or even extrapolations
174 to the basis set limit must be used for this task [12].

175 Due to the fact that this is computationally too expensive for engineering
176 purposes, we used the parameters for the dispersive and repulsive interactions
177 for an initial model from similar sites of other molecular models. Some of these
178 parameters were subsequently fitted in the optimization process to yield the
179 correct VLE behavior of the modeled substance.

3 Optimization to VLE data

181 The optimization was performed using a Newton scheme as proposed by
182 Stoll [32]. The applied method has many similarities with the one published by
183 Ungerer et al. [33] and later on modified by Bourasseau et al. [34]. It relies
184 on a least-square minimization of a weighted fitness function \mathcal{F} that quantifies
185 the deviations of simulation results from a given molecular model compared to
186 experimental data. The weighted fitness function writes as

$$\mathcal{F} = \frac{1}{d} \sum_{i=1}^d \frac{1}{(\delta A_{i,\text{sim}})^2} (A_{i,\text{sim}}(\mathbf{M}_0) - A_{i,\text{exp}})^2, \quad (4)$$

188 wherein the n -dimensional vector $\mathbf{M}_0 = (m_{0,1}, \dots, m_{0,n})$ represents the set of n

189 model parameters $m_{0,1}, \dots, m_{0,n}$ to be optimized. The deviations of results from
 190 simulation $A_{i,\text{sim}}$ to experimental data $A_{i,\text{exp}}$ are weighted with the expected
 191 simulation uncertainties $\delta A_{i,\text{sim}}$. Equation (4) allows simultaneous adjustment
 192 of the model parameters to different thermophysical properties A_i (saturated
 193 liquid densities ρ' , vapor pressures p_σ , and enthalpies of vaporization Δh_v at
 194 various temperatures in the present work).

195 The unknown functional dependence of the property A_i on the model pa-
 196 rameters is approximated by a first order Taylor series developed in the vicinity
 197 of the initial parameter set \mathbf{M}_0

$$A_{i,\text{sim}}(\mathbf{M}_{\text{new}}) = A_{i,\text{sim}}(\mathbf{M}_0) + \sum_{j=1}^n \frac{\partial A_{i,\text{sim}}}{\partial m_j} \cdot (m_{\text{new},j} - m_{0,j}) . \quad (5)$$

199 Therein, the partial derivatives of A_i with respect to each model parameter m_j ,
 200 i.e. the sensitivities, are calculated from difference quotients

$$\frac{\partial A_{i,\text{sim}}}{\partial m_j} \approx \frac{A_{i,\text{sim}}(m_{0,1}, \dots, m_{0,j} + \Delta m_j, \dots, m_{0,n}) - A_{i,\text{sim}}(m_{0,1}, \dots, m_{0,j}, \dots, m_{0,n})}{\Delta m_j} . \quad (6)$$

202 Assuming a sound choice of the model parameter variations Δm_j , i.e. small
 203 enough to ensure linearity and large enough to yield differences in the simulation
 204 results significantly above the statistical uncertainties, this method allows a step-
 205 wise optimization of the molecular model by minimization of the fitness function
 206 \mathcal{F} . Experience shows that an optimized set of model parameters was usually
 207 found within a few iterative steps when starting from a reasonable initial model.

208 Correlations for vapor pressure, saturated liquid density, and enthalpy of
 209 vaporization, taken from the DIPPR database [35], were used as "experimental
 210 data" for model adjustment and evaluation. This was done even in cases where
 211 the correlation is based on no or only few true experimental data points, as the
 212 correlations were regarded best practice. The comparison between simulation
 213 results and experiment was done by applying fits to the simulation data accord-
 214 ing to Lotfi et al. [36]. The relative deviation between fit and correlation was
 215 calculated in steps of 1 K from 55 to 97% of the critical temperature and is
 216 denoted by "mean unsigned error" in the following.

217 Vapor-liquid equilibrium simulations were performed using the Grand Equi-
218 librium method by Vrabec et al. [37], technical simulation details are given in
219 the appendix.

220 **4 Molecular Models**

221 The selected ten molecules belong to different substance classes to show the
222 wide applicability of the proposed strategy. In the present work, we restricted
223 ourselves to small molecules, where the internal degrees of freedom may be
224 neglected. Thus, the molecular models are rigid, using the most stable configu-
225 ration determined by QM.

226 The optimized parameter sets of the new molecular models are summarized
227 in Table 1. Table 2 compares the critical properties from simulation to exper-
228 imental data. The critical properties from simulation were obtained through
229 fits to VLE simulation results as suggested by Lotfi et al. [36]. The estimated
230 uncertainties of critical temperature, critical density, and critical pressure from
231 simulation are 0.5, 2, and 2%, respectively. A very good agreement between sim-
232 ulation and experiment was reached, being predominantly within the combined
233 error bars.

234 In the following sections, substance specific details are briefly discussed.
235 Furthermore, references to alternative models from the literature are given and
236 the simulation results from the present models are compared to simulation data
237 from the literature where available. Numerical VLE simulation results are given
238 as Supplementary Material.

239 **4.1 Iso-Butane and Cyclohexane**

240 The branched alkane iso-butane and the cyclic alkane cyclohexane show only
241 very weak static polarities. Here, the main contributions to the intermolecular
242 interaction are dispersion and repulsion. The electrostatic interactions have
243 only a minor influence but should not be neglected completely.

244 In the literature different molecular models for iso-butane can be found,

245 which are mostly based on force fields for branched alkanes. The well-known
246 OPLS force field by Jorgensen et al. is available in two versions for iso-butane,
247 one using the united-atom approach [45] and one using an all-atom description
248 [46]. Both OPLS force fields were optimized to liquid density and enthalpy of
249 vaporization at 293 K only. The model of Poncela et al. [47] was adjusted
250 to yield correct second virial coefficients. For a better applicability in a wider
251 range of states, recent developments were optimized to experimental VLE data.
252 Examples from this group are the force fields presented by Nath and de Pablo
253 [48], Martin and Siepmann [49], Bourasseau et al. [50], or Chang and Sandler
254 [51].

255 For the present model, four LJ sites, one for each methyl group and one
256 for the methine group, were used to describe dispersion and repulsion of iso-
257 butane. The polarity was modeled by a single (weak) dipole (0.1347 D) located
258 in the center of mass. Orientation and magnitude of the dipole were taken from
259 the QM calculation. For the initial model, the LJ parameters were taken from
260 Ungerer et al. [15]. It was sufficient to adjust a single parameter, the offset
261 distance of the methine group. It was optimized to 0.4 of the carbon-hydrogen
262 distance, cf. Figure 1 and held constant subsequently. The parameters of the
263 present model are given in Table 1.

264 Figures 2 to 4 show saturated densities, vapor pressure, and enthalpy of
265 vaporization, respectively, from the present iso-butane model in comparison to
266 experimental data [35]. Figure 5 shows a deviation plot between simulation and
267 experimental data. In the deviation plot also simulation results from Martin
268 and Siepmann, using their TraPPE force field, [49] and from Nath and de Pablo
269 [48] are included. A very good agreement was obtained for the present model
270 yielding mean unsigned errors in vapor pressure, saturated liquid density, and
271 enthalpy of vaporization of 4.2, 0.6, and 1.8%, respectively, in the temperature
272 range from 55 to 97% of the critical temperature, which is about 225 to 395 K.
273 For vapor pressure, the present model yields significantly better results than
274 the TraPPE force field, while no simulation data is available from Nath and

275 de Pablo for this property. For saturated liquid density, all three models yield
276 comparable results within 1% deviation to experimental data. No comparison
277 between the models was possible for enthalpy of vaporization due to missing
278 numerical data in [48, 49].

279 For cyclohexane different molecular models are available in the literature [52,
280 53, 54, 55] which all account for the internal degrees of freedom. Nevertheless,
281 the present cyclohexane model was assumed to be rigid and in its most stable
282 configuration, i.e. the saddle shape. The molecular model consists of six LJ
283 sites, one for each methylene group. The static polarity was modeled by a
284 single quadrupole parameterized according to QM. The two LJ parameters for
285 methylene were optimized to experimental VLE data. The parameters of the
286 present model are given in Table 1.

287 Figures 2 to 4 again show present VLE simulation results in comparison to
288 experimental data for cyclohexane. Figure 6 shows the deviation plot including
289 simulation results from Bourasseau et al. [50]. The mean unsigned errors in
290 vapor pressure, saturated liquid density, and enthalpy of vaporization for the
291 present model are 0.9, 0.5, and 5.6%, respectively. Simulation results for the
292 enthalpy of vaporization show systematic relative deviations towards the critical
293 point, while the absolute deviation is below 2.5 kJ/mol.

294 Compared to the model of Bourasseau et al. improvements in the descrip-
295 tion of the saturated liquid density were achieved. The simulation results for
296 vapor pressure agree within their assumed simulation uncertainties which were
297 not reported by Bourasseau et al. An interesting point is that both molecular
298 models yield the same deviations from experimental data on the enthalpy of
299 vaporization, while the DIPPR database reports true experimental data up to
300 $0.97T_c$. For all other molecular models for cyclohexane mentioned above, no nu-
301 merical VLE simulation data is reported in the literature. Thus, no comparison
302 is made here.

4.2 Formaldehyde and Dimethyl Ether

304 The present molecular model for formaldehyde consists of two LJ sites, one
305 for the oxygen atom and one for the methylene group, as well as one dipole. The
306 dipole is located in the center of mass and its moment was specified according to
307 QM results, cf. Table 1. All four LJ parameters were adjusted to experimental
308 VLE data and are given in Table 1.

309 Figures 7 to 8 compare simulation results and experimental VLE data for
310 formaldehyde, Figure 9 shows the relative deviations. Mean unsigned errors in
311 vapor pressure, saturated liquid density, and enthalpy of vaporization are 4.3,
312 0.9, and 8.4%, respectively.

313 Note that, in contrast to iso-butane or cyclohexane, the available experimen-
314 tal data base is very weak here. In fact, for vapor pressure only a single data set
315 from the year 1935 [56] is available. For saturated liquid density and enthalpy
316 of vaporization, respectively, a single data point at 254 K is “accepted” by the
317 DIPPR database [35]. Thus, no further optimization of the molecular model was
318 attempted although the desired quality seems not to be fully reached. Hermida-
319 Raón and Ríos [57] published a molecular model based on QM calculations of
320 formaldehyde dimers and trimers. They applied their model to liquid phase
321 simulations but report no results on VLE properties. Thus, no comparison is
322 presented here.

323 Dimethyl ether was modeled with three LJ sites in the present work, one
324 for the oxygen atom and one for each methyl group. A dipole was located in
325 the center of mass and oriented along the symmetry axis of the molecule, where
326 the dipole moment was again taken from QM calculation. For an initial model,
327 the same LJ parameters of the methyl groups were taken as for the iso-butane
328 model, i.e. those by Ungerer et al. [15]. An adjustment of the two LJ parameters
329 of the oxygen site was sufficient to reach the desired quality. Alternative models
330 for dimethyl ether are given in [58, 59, 60, 61].

331 The simulation results for the present model of dimethyl ether in comparison

332 to the experimental VLE data are shown in Figures 2 to 4. Figure 10 shows the
333 relative deviations between simulation and experiment also including simulation
334 results from Stubbs et al. [60] and very recent results from Ketko and Potoff [61].
335 For dimethyl ether a good experimental data base is available for optimization
336 of the molecular model. The simulation data of the present model is in very
337 good agreement with the correlations of experimental data. The mean unsigned
338 errors in vapor pressure, saturated liquid density, and enthalpy of vaporization
339 are 2.6, 0.4, and 1.0%, respectively.

340 For vapor pressure, both molecular models specifically adjusted to dimethyl
341 ether, i.e. the present model and the model by Ketko and Potoff, yield better re-
342 sults than the transferable molecular model by Stubbs et al., while for saturated
343 density all models perform similarly. For enthalpy of vaporization, the present
344 model and the model by Ketko and Potoff also yield comparable results. Note
345 that the parameters for the electrostatic interactions of the model by Ketko and
346 Potoff were adjusted to experimental VLE data as well.

347 It can be summarized that the model by Ketko and Potoff [61] and the
348 present dimethyl ether model are of similar quality and outperform the trans-
349 ferable model by Stubbs et al. [60]. While Ketko and Potoff adjusted four
350 LJ parameters and the point charge magnitudes for their electrostatic inter-
351 actions, following the proposed modeling strategy an optimization of only two
352 Lennard-Jones parameters was sufficient to reach the same quality.

4.3 Sulfur Dioxide, Dimethyl Sulfide, and Thiophene

354 For sulfur dioxide, a molecular model was published by Sokolić et al. [62,
355 63] which was optimized to total energy and pressure in the liquid state. It
356 was recently reviewed by Ribeiro [64]. Alternatively, the commercial force field
357 COMPASS [65] reports parameters for sulfur dioxide.

358 For the present molecular model, the intermolecular interactions of sulfur
359 dioxide were modeled with three LJ sites, i.e. one per atom, plus one dipole and
360 one quadrupole. The electrostatic sites are located in the center of mass and

361 parameterized according to the results of QM calculation. The four parameters
362 of the LJ sites, i.e. σ_S , ε_S , σ_O , and ε_O , were adjusted to experimental VLE
363 data. All parameters of the molecular model are given in Table 1.

364 Present simulation results for sulfur dioxide are compared to experimental
365 VLE data in Figures 11 to 13. Figure 9 shows the relative deviations between
366 simulation and experiment for the present model, while no numerical VLE sim-
367 ulation data for sulfur dioxide from other authors was available to us. Mean
368 unsigned errors in vapor pressure, saturated liquid density, and enthalpy of va-
369 porization are 4.0, 0.9, and 1.6%, respectively. The good experimental data
370 base, with more than 60 individual experimental VLE data points, allows a
371 thorough optimization of the molecular model to the desired quality.

372 Literature models for dimethyl sulfide are given in [66, 67, 68]. The present
373 dimethyl sulfide model consists of three LJ sites, one for the sulfur atom and one
374 for each methyl group. The electrostatic interactions are modeled by one dipole
375 and two quadrupoles oriented perpendicularly to each other. This description
376 of the electrostatics was chosen, as QM yields a charge distribution, which can
377 not properly be described with a lower number of electrostatic sites. The LJ
378 parameters of the methyl groups were assumed to be the same as for iso-butane
379 and dimethyl oxide, while the parameters of the sulfur group were adjusted to
380 experimental VLE data.

381 Figures 11 to 13 show the present simulation results for dimethyl sulfide in
382 comparison to experimental VLE data. Figure 14 shows the relative deviations
383 between simulation and experiment for the present model and for the model of
384 Lubna et al. [68]. Note that simulation results on enthalpy of vaporization were
385 not included in [68]. For the present model of dimethyl sulfide, mean unsigned
386 errors in vapor pressure, saturated liquid density, and enthalpy of vaporization
387 are 4.0, 0.7, and 3.8%, respectively. Particularly the vapor pressure is better
388 described than by the model of Lubna et al.

389 Also thiophene was described in the present work by a rigid model in its
390 most stable conformation, as for cyclohexane. Five LJ sites, one for each of the

391 four methylene groups and one for the sulfur atom, as well as one dipole and
392 one quadrupole were used. The electrostatic parameters were directly passed
393 on from QM. A total of four LJ parameters, i.e. σ_{CH_2} , $\varepsilon_{\text{CH}_2}$, σ_{S} , and ε_{S} ,
394 were adjusted to experimental VLE data. The optimized parameters are given
395 in Table 1. Alternative molecular models for thiophene can be found in the
396 literature [68, 69, 70]

397 Figures 11 to 13 compare simulation results to experimental VLE data for
398 thiophene, while the relative deviations are shown in Figure 15. In the deviation
399 plot also simulation results from Lubna et al. [68], Juárez-Guerra et al. [69],
400 and Pérez-Pellitero et al. [70] are included. Mean unsigned errors of the present
401 model in vapor pressure, saturated liquid density, and enthalpy of vaporization
402 are 3.8, 1.2, and 3.2%, respectively.

403 The thiophene model by Juárez-Guerra et al. [69] shows significant devia-
404 tions in both vapor pressure and saturated liquid density while no simulation re-
405 sults for the enthalpy of vaporization were given by the authors. The anisotropic
406 united atoms (AUA) potential by Pérez-Pellitero et al. [70] overpredicts the va-
407 por pressure over the complete temperature range by up to 20%. Simulation
408 results for saturated liquid density and enthalpy of vaporization are in very good
409 agreement with the DIPPR correlation for low temperatures but give noticeably
410 higher values than the DIPPR correlation for temperatures above $0.7T_c$. The
411 TraPPE force field by Lubna et al. [68] yields vapor pressure results that agree
412 very well with the DIPPR correlation and the simulation results within their
413 scatter. Saturated densities are higher than the correlation towards the critical
414 point for all four molecular models. For enthalpy of vaporization no numerical
415 data were given by Lubna et al.

416 It should be noted that for thiophene experimental vapor pressure data is
417 available for temperatures up to around $0.9 T_c$, experimental saturated liquid
418 densities and enthalpies of vaporization are only available up to approximately
419 $0.63 T_c$. Thus, an assessment of the different molecular models regarding density
420 and enthalpy of vaporization above $0.7 T_c$ on the basis of the DIPPR correlations

421 is questionable.

4.4 Hydrogen Cyanide, Acetonitrile, and Nitromethane

423 Hydrogen cyanide was modeled in the present work with two LJ sites, one
424 for the methine group and one for the nitrogen atom. Electrostatic interactions
425 were modeled by one dipole and one quadrupole oriented along the symmetry
426 axis, where the parameters were passed on from QM. All four LJ parameters
427 were adjusted to experimental VLE data. The optimized parameters can be
428 found in Table 1. For hydrogen cyanide no other molecular models were found
429 in the literature.

430 Figures 11 to 13 compare simulation results and experimental VLE data for
431 hydrogen cyanide. Figure 9 shows the relative deviations. Unfortunately, the
432 DIPPR database [35] contains no true experimental data on the enthalpy of
433 vaporization for hydrogen cyanide. Consequently, in the optimization process,
434 only minor attention was paid to the enthalpy of vaporization. Mean unsigned
435 errors in vapor pressure, saturated liquid density, and enthalpy of vaporization
436 are nominally 7.2, 1.0, and 12.2%, respectively.

437 Several molecular models for acetonitrile are available in the literature. Jor-
438 gensen and Briggs [71], Price et al. [77], Guárdia et al. [72], and Nikitin and
439 Lyubartsev [73] present models that were optimized to the liquid density and
440 enthalpy of vaporization at 293 K. Hloucha and Deiters [74] give a polarizable
441 molecular model for simulations in the liquid state while Hloucha et al. [29]
442 published a model that is based on *ab initio* calculations. Finally, Wick et al.
443 [78] proposed an extension of their TraPPE force field that was optimized to
444 VLE data to cover acetonitrile.

445 In the present work, acetonitrile was modeled using three LJ sites, one for the
446 methyl group, one for the central carbon atom, and one for the nitrogen atom.
447 The electrostatic interactions were modeled by one dipole and one quadrupole,
448 located in the center of mass and parameterized strictly according to QM results.
449 The parameters of the LJ sites of the methyl group and the nitrogen atom were

450 adjusted to experimental VLE data. The LJ parameters of the central carbon
451 atom were taken from unpublished work on carbon dioxide and excluded from
452 optimization, only a very weak sensitivity of the VLE simulation results on
453 these parameters was found. All parameters of the molecular model are given
454 in Table 1.

455 Simulation results for acetonitrile are compared to experimental VLE data
456 in Figures 7 to 8. The relative deviations between simulation and experiment
457 are shown in Figure 16 next to results of the OPLS-UA force field by Jorgensen
458 and Briggs [71] and the TraPPE force field by Wick et al., which were reported
459 for both models in [78]. Despite the good experimental data base, the desired
460 quality was not achieved by the present optimization. Only a fair description
461 of the experimental VLE was reached. Mean unsigned errors in vapor pressure,
462 saturated liquid density, and enthalpy of vaporization are 19.7, 0.9, and 5.4%,
463 respectively.

464 The large relative deviations in vapor pressure result from systematic un-
465 derestimations at low temperatures. In this region also difficulties were encoun-
466 tered in the simulative calculation of the chemical potential in the liquid phase
467 to determine the phase equilibrium. This was even the case when the more so-
468 phisticated gradual insertion method [79] was used, as described in the appendix
469 in greater detail.

470 The OPLS-UA force field by Jorgensen and Briggs [71] significantly overes-
471 timates the vapor pressure of acetonitrile and shows deviations in the saturated
472 liquid density up to 4%, cf. Figure 16. Simulation results for vapor pressure
473 obtained with the TraPPE force field by Wick et al. [78] show a very good
474 agreement with the DIPPR correlation, while the saturated density is slightly
475 overpredicted towards the critical point. No comparison of the literature models
476 for acetonitrile is possible regarding the enthalpy of vaporization due to the lack
477 of numerical simulation results.

478 The present molecular model for nitromethane consists of four LJ sites, one
479 for the methyl group, one for the nitrogen atom, and one for the two oxygen

480 atoms each. The electrostatic interactions were modeled by one dipole and
481 one quadrupole oriented along the symmetry axis, where the parameters were
482 specified according to QM results. All six LJ parameters were adjusted to
483 experimental VLE data. Alternative models are available in the literature [75,
484 76, 77, 78].

485 Figures 11 to 13 compare the present simulation results for nitromethane
486 with experimental VLE data. Figure 17 shows the relative deviations obtained
487 with the present model, the OPLS-AA force field by Price et al. [77], and the
488 TraPPE force field by Wick et al. [78]. For the present model of nitromethane,
489 mean unsigned errors in vapor pressure, saturated liquid density, and enthalpy
490 of vaporization are 18.7, 0.2, and 7.0%, respectively. Again, a systematic un-
491 derprediction of the vapor pressure at low temperatures was found, leading to
492 the high relative deviations, as for acetonitrile.

493 The OPLS-AA force field overpredicts the vapor pressure by about 80% and
494 underpredicts the saturated liquid density by up to 6%. The TraPPE force field
495 of Wick et al. that was optimized to experimental VLE data, yields very good
496 results in vapor pressure for low temperatures while the result for the highest
497 simulated temperature deviates by +34% from the DIPPR correlation. Regard-
498 ing saturated liquid density, strong scatter and large statistical uncertainties of
499 the simulation results are observed for both literature models.

500 **5 Conclusion**

501 A strategy was proposed for the rapid development of molecular models
502 for engineering applications. The strategy relies on results from QM *ab initio*
503 calculations to include physically sound molecular properties and to reduce the
504 number of adjustable parameters. Dispersive and repulsive interactions were
505 modeled by LJ sites. Thus, the LJ interaction sites were located according
506 to atom positions obtained by QM energy minimization on Hartree-Fock level.
507 For the parameterization of the electrostatic interactions, QM calculations were
508 performed using the Møller-Plesset 2 level of theory and the COSMO method.

509 The resulting electron density distribution was reduced to ideal point dipoles
510 and ideal linear point quadrupoles located in the center of mass. The moments
511 and orientations of the dipoles and quadrupoles were passed on to the molecular
512 models without any modification.

513 A united-atom approach was used for methine, methylene, and methyl groups
514 to reduce the total number of interaction sites. The parameters of the LJ sites
515 were initially taken from similar sites of other molecular models and were sub-
516 sequently optimized to reproduce experimental VLE data, i.e. vapor pressure,
517 saturated liquid density, and enthalpy of vaporization. It was aimed to achieve
518 deviations between simulation and experiment of below 5, 1, and 5% in vapor
519 pressure, saturated liquid density, and enthalpy of vaporization, respectively.

520 The new modeling strategy was successfully applied to ten molecules from
521 different substances classes, i.e. iso-butane, cyclohexane, formaldehyde, dimethyl
522 ether, sulfur dioxide, dimethyl sulfide, thiophene, hydrogen cyanide, acetonitrile,
523 and nitromethane. Simulation results for the different substances agree
524 well with correlations of experimental data taken from the DIPPR database
525 [35], with noticeable deviations in the vapor pressure at low temperatures for
526 acetonitrile and nitromethane.

527 For the two elongated molecules acetonitrile and nitromethane, the reduction
528 of the electrostatic interactions to sites located in the center of mass seems to be
529 an over-simplification, as the optimization of the molecular models was not fully
530 successful. Also an adjustment of the electrostatic parameters, while keeping
531 the ratio of the polar moments constant (not reported here in detail), did not
532 yield significant improvements in the quality of the molecular models. A further
533 study, e.g. using two or more spatially distributed electrostatic sites, is beyond
534 the scope of this paper.

535 For all other molecules a significant improvement compared to available
536 molecular models from the literature was achieved. Through an optimization
537 to substance specific experimental VLE data, a very good description of the
538 phase equilibria was obtained. Furthermore, in case of dimethyl ether it was

539 shown that with the proposed modeling strategy it was possible to reach the
540 same model quality by optimization of just two model parameters compared to
541 five optimized parameters for the model by Ketko and Potoff [61].

56 Acknowledgment

543 The authors gratefully acknowledge financial support by Deutsche Forschungs-
544 gemeinschaft, Schwerpunktprogramm 1155 "Molecular Modeling and Simula-
545 tion in Process Engineering". The simulations were performed the national su-
546 per computer NEC SX-8 at the High Performance Computing Center Stuttgart
547 (HLRS) under the grant MMHBF and on the HP XC6000 super computer at
548 the Steinbuch Centre for Computing, Karlsruhe under the grant MMSTP.

549 The authors want to thank Inga Utz for her modeling work on the sulfur
550 and nitrogen containing compounds.

57 Appendix

552 The Grand Equilibrium method [37] was used to calculate VLE data at seven
553 to thirteen temperatures from 50 to 97% of the critical temperature during
554 the optimization process. For the liquid, molecular dynamics simulations were
555 performed in the isobaric-isothermal (NpT) ensemble using isokinetic velocity
556 scaling [8] and Anderson's barostat [80]. There, the number of molecules was 864
557 throughout and the time step was 1 to 3 fs depending on the molecular weight
558 and the magnitude of the intermolecular interactions. The initial configuration
559 was a face centered cubic lattice, the fluid was equilibrated over 25 000 time
560 steps with the first 5 000 time steps in the canonical (NVT) ensemble. The
561 production run time span was 150 000 to 200 000 time steps with a membrane
562 mass of 10^9 kg/m⁴. Widom's insertion method [81] was used to calculate the
563 chemical potential by inserting up to 4 000 test molecules every production time
564 step.

565 In cases where Widom's insertion method yielded large statistical uncertain-
566 ties for the chemical potential, i.e. at high densities for strongly interacting

567 molecules, Monte Carlo simulations were performed in the NpT ensemble for
568 the liquid. Then, the chemical potential was calculated by the gradual inser-
569 tion method [82, 79]. The number of molecules was 500. Starting from a face
570 centered cubic lattice, 15 000 Monte Carlo cycles were performed for equilibra-
571 tion and 50 000 for production, each cycle containing 500 translation moves,
572 500 rotation moves, and 1 volume move. Every 50 cycles, 5000 fluctuating
573 state change moves, 5000 fluctuating particle translation/rotation moves, and
574 25000 biased particle translation/rotation moves were performed, to determine
575 the chemical potential. These computationally demanding simulations yield the
576 chemical potential in dense and strong interacting liquids with high accuracy,
577 leading to reasonable uncertainties in the VLE.

578 For the corresponding vapor, Monte Carlo simulations in the pseudo- μVT
579 ensemble were performed. The simulation volume was adjusted to lead to an
580 average number of 500 molecules in the vapor phase. After 1 000 initial NVT
581 Monte Carlo cycles, starting from a face centered cubic lattice, 10 000 equi-
582 libration cycles in the pseudo- μVT ensemble were performed. The length of
583 the production run was 50 000 cycles. One cycle is defined here to be a num-
584 ber of attempts to displace and rotate molecules equal to the actual number of
585 molecules plus three insertion and three deletion attempts.

586 The cut-off radius was set to 17.5 Å throughout and a center of mass cut-off
587 scheme was employed. Lennard-Jones long-range interactions beyond the cut-
588 off radius were corrected employing angle averaging as proposed by Lustig [83].
589 Electrostatic interactions were approximated by a resulting molecular dipole
590 and corrected using the reaction field method [8]. Statistical uncertainties in
591 the simulated values were estimated by a block averaging method [84].

592 **References and Notes**

- 593 (1) Ungerer, P.; Nieto-Draghi, C.; Rousseau, B.; Ahunbay, G.; Lachet, V. *J.*
594 *Mol. Liq.* **2007**, *134*, 71–89.

- 595 (2) Ungerer, P.; Nieto-Draghi, C.; Lachet, V.; Wender, A.; Di Lella, A.;
596 Boutin, A.; Rousseau, B.; Fuchs, A.H. *Mol. Sim.*, **2007**, *33*, 15–30.
- 597 (3) Martin, M.G. *Fluid Phase Equilib.*, **2006**, *248*, 50–55.
- 598 (4) Eckl, B.; Vrabec, J.; Hasse, H. *Fluid Phase Equilib.* **2008**, to appear.
- 599 (5) Eckl, B.; Vrabec, J.; Hasse, H. *Mol. Phys.* **2008**, accepted.
- 600 (6) Jones, J.E. *Proc. Roy. Soc.* **1924**, *106A*, 441–462.
- 601 (7) Jones, J.E. *Proc. Roy. Soc.* **1924**, *106A*, 463–477.
- 602 (8) Allen, M.P.; Tildesley, D.J. *Computer simulations of liquids*; Clarendon
603 Press: Oxford, 1987.
- 604 (9) Gray, C.G.; Gubbins, K.E. *Theory of molecular fluids. 1. Fundamentals*;
605 Clarendon Press: Oxford, 1984.
- 606 (10) Lorentz, H.A. *Ann. d. Phys.* **1881**, *12*, 127–136.
- 607 (11) Berthelot, D. *Compt. Rend. Ac. Sc.* **1889**, *126*, 1703–1706.
- 608 (12) Sandler, S.I.; Castier, M. *Pure Appl. Chem.* **2007**, *79*, 1345–1359.
- 609 (13) Schmidt, M.W.; Baldrige, K.K.; Boatz, J.A.; Elbert, S.T.; Gordon, M.S.;
610 Jensen, J.H.; Koseki, S.; Matsunaga, N.; Nguyen, K.A.; Shujun, S.; Win-
611 dus, T.L.; Dupuis, M.; Montgomery, A.M. *J. Comput. Chem.* **1993**, *14*,
612 1347–1363.
- 613 (14) Leach, A.R. *Molecular Modeling. Principles and Application*; 2nd ed.;
614 Prentice-Hall: Englewood Cliffs, 2001.
- 615 (15) Ungerer, P.; Beauvais, C.; Delhommelle, J.; Boutin, A.; Rousseau, B.;
616 Fuchs, A.H. *J. Chem. Phys.* **2000**, *112*, 5499–5510.
- 617 (16) Klamt, A. *J. Phys. Chem.* **1995**, *99*, 2224–2235.
- 618 (17) Chirlian, L.E.; Francl, M.M. *J. Comput. Chem.* **1987**, *8*, 894–905.

- 619 (18) Breneman, C.M.; Wiberg, K.B. *J. Comput. Chem.* **1990**, *11*, 361–373.
- 620 (19) Stone, A.J.; Alderton, M. *Mol. Phys.* **2002**, *100*, 221–233.
- 621 (20) Eggenberger, R.; Gerber, S.; Huber, H.; Welker, M. *Mol. Phys.* **1994**, *82*,
622 689–699.
- 623 (21) Vogt, P.S.; Liapine, R.; Kirchner, B.; Dyson, A.J.; Huber, H.; Marcelli,
624 G.; Sados, R.J. *Phys. Chem. Chem. Phys.* **2001**, *3*, 1297–1302.
- 625 (22) Garrison, S.L.; Sandler, S.I. *J. Chem. Phys.* **2002**, *117*, 10571–10580.
- 626 (23) Nasrabad, A.E.; Laghaei, R.; Deiters, U.K. *J. Chem. Phys.* **2004**, *121*,
627 6423–6434.
- 628 (24) Ermakova, E.; Solca, J.; Huber, H.; Welker, M. *J. Chem. Phys.* **1995**, *102*,
629 4942–4951.
- 630 (25) Nasraba, A.E.; Deiters, U.K. *J. Chem. Phys.* **2003**, *119*, 947–952.
- 631 (26) Leonhar, K.; Deiters, U.K. *Mol. Phys.* **2002**, *100*, 2571–2585.
- 632 (27) Welker, M.; Steinebrunner, G.; Solca, J.; Huber, H. *Chem. Phys.* **1996**,
633 *213*, 253–261.
- 634 (28) Naicker, P.K.; Sum, A.K.; Sandler, S.I. *J. Chem. Phys.* **2003**, *118*, 4086–
635 4093.
- 636 (29) Hloucha, M.; Sum, A.K.; Sandler, S.I. *J. Chem. Phys.* **2000**, *113*, 5401–
637 5406.
- 638 (30) Garrison, S.L.; Sandler, S.I. *J. Phys. Chem.* **2004**, *108*, 18972–18979.
- 639 (31) Garrison, S.L.; Sandler, S.I. *J. Chem. Phys.* **2005**, *123*, 054506.
- 640 (32) Stoll, J. *Molecular Models for the Prediction of Thermophysical Properties*
641 *of Pure Fluids and Mixtures*; Fortschritt-Berichte VDI, Reihe 3, 836; VDI-
642 Verlag: Düsseldorf, 2005.

- 643 (33) Ungerer, P.; Boutin, A.; Fuchs, A.H. *Mol. Phys.* **1999**, *97*, 523–539.
- 644 (34) Bourasseau, E.; Haboudou, M.; Boutin, A.; Fuchs, A.H.; Ungerer, P. *J.*
645 *Chem. Phys.* **2003**, *118*, 3020–3034.
- 646 (35) Rowley, R.L.; Wilding, W.V.; Oscarson, J.L.; Yang, Y.; Zundel, N.A.;
647 Daubert, T.E.; Danner, R.P. *DIPPR*[®] *Data Compilation of Pure Com-*
648 *pound Properties*; Design Institute for Physical Properties, AIChE: New
649 York, 2006.
- 650 (36) Lotfi, A.; Vrabec, J.; Fischer, J. *Mol. Phys.* **1992**, *76*, 1319–1333.
- 651 (37) Vrabec, J.; Hasse, H. *Mol. Phys.* **2002**, *100*, 3375–3383.
- 652 (38) Daubert, T.E. *J. Eng. Chem. Data* **1996**, *41*, 365–372.
- 653 (39) Reid, R.C.; Prausnitz, J.M.; Sherwood, T.K. *The Properties of Gases and*
654 *Liquids*; 3rd ed.; McGraw-Hill: New York, 1977.
- 655 (40) Kudchadker, A.P.; Ambrose, A.; Tsonopoulos, C. *J. Chem. Eng. Data*
656 **2001**, *46*, 457–479.
- 657 (41) Mathews, J.F. *Chem. Rev.* **1972**, *72*, 71–100.
- 658 (42) Tsonopoulos, C.; Ambrose, D. *J. Chem. Eng. Data* **2001**, *46*, 480–485.
- 659 (43) Marsh, K.N.; Young, C.L.; Morton, D.W.; Ambrose, D.; Tsonopoulos, C.
660 *J. Chem. Eng. Data* **2006**, *51*, 305–314.
- 661 (44) Kudchadker, A.P.; Alani, G.H.; Zwolinski, B.J. *Chem. Rev.* **1968**, *68*,
662 659–735.
- 663 (45) Jorgensen, W.L.; Madura, J.D.; Swenson, C.J. *J. Am. Chem. Soc.* **1984**,
664 *106*, 6638–6646.
- 665 (46) Jorgensen, W.L.; Maxwell, D.S.; Tirado-Rives, J. *J. Am. Chem. Soc.*
666 **1996**, *118*, 11225–11236.
- 667 (47) Poncela, A.; Rubio, A.M.; Freire, J.J. *Mol. Phys.* **1997**, *91*, 189–201.

- 668 (48) Nath, S.K.; de Pablo, J.J. *Mol. Phys.* **2000**, *98*, 231–238.
- 669 (49) Martin, M.G.; Siepmann, J.I. *J. Phys. Chem. B* **1999**, *103*, 4508–4517.
- 670 (50) Bourasseau, E.; Ungerer, P.; Boutin, A.; Fuchs, A.H. *Mol. Sim.* **2002**, *28*,
671 317–336.
- 672 (51) Chang, J.; Sandler, S.I. *J. Chem. Phys.* **2004**, *121*, 7474–7483.
- 673 (52) Errington, J.R.; Panagiotopoulos, A.Z. *J. Chem. Phys.* **1999**, *111*, 9731–
674 9738.
- 675 (53) Neubauer, B.; Boutin, A.; Tavitan, B.; Fuchs, A.H. *Mol. Phys.* **1999**, *97*,
676 769–776.
- 677 (54) Faller, R.; Schmitz, H.; Biermann, O.; Müller-Plathe, F. *J. Comput. Chem.*
678 **1999**, *20*, 1009–1017.
- 679 (55) Bourasseau, E.; Ungerer, P.; Boutin, A. *J. Phys. Chem. B* **2002**, *106*,
680 5483–5491.
- 681 (56) Spence, R.; Wild, W. *J. Chem. Soc.* **1935**, *1*, 506–509.
- 682 (57) Hermida-Raón, J.M.; Ríos, M.A. *J. Phys. Chem. A* **1998**, *102*, 10818–
683 10827.
- 684 (58) Jorgensen, W.L. *J. Am. Chem. Soc.* **1981**, *103*, 335–340.
- 685 (59) Lin, B.; Halley, J.W. *J. Phys. Chem.* **1995**, *99*, 16474–16478.
- 686 (60) Stubbs, J.M.; Potoff, J.J.; Siepmann, J.I. *J. Phys. Chem. B* **2004**, *108*,
687 17596–17605.
- 688 (61) Ketko, M.B.H.; Potoff, J.J. *Mol. Sim.* **2007**, *33*, 769–776.
- 689 (62) Sokolić, F.; Guissani, Y.; Guillot, B. *Mol. Phys.* **1985**, *56*, 239–253.
- 690 (63) Sokolić, F.; Guissani, Y.; Guillot, B. *J. Phys. Chem.* **1985**, *89*, 3023–3026.
- 691 (64) Ribeiro, M.C.C. *J. Phys. Chem. B* **2006**, *110*, 8789–8797.

- 692 (65) Yang, J.; Ren, Y.; Tian, A. *J. Phys. Chem. B* **2000**, *104*, 4951–4957.
- 693 (66) Jorgensen, W.L. *J. Phys. Chem.* **1986**, *90*, 6379–6388.
- 694 (67) Delhommelle, J.; Tschirwitz, C.; Ungerer, P.; Granucci, G.; Millié, P.;
695 Pattou, D.; Fuchs, A.H. *J. Phys. Chem. B* **2000**, *104*, 4745–4753.
- 696 (68) Lubna, N.; Kamath, G.; Potoff, J.J.; Rai, N.; Siepmann, J.I. *J. Phys.*
697 *Chem. B* **2005**, *109*, 24100–24107.
- 698 (69) Juárez-Guerra, F.; Rivera, J.L.; Zúñiga-Moreno, A.; Galicia-Luna, L.A.;
699 Rico, J.L.; Lara, J. *Sep. Sci. Technol.* **2006**, *41*, 261–281.
- 700 (70) Pérez-Pellitero, J.; Ungerer, P.; Mackie, A.D. *J. Phys. Chem. B* **2007**,
701 *111*, 4460–4466.
- 702 (71) Jorgensen, W.L.; Briggs, J.M. *Mol. Phys.* **1988**, *63*, 547–558.
- 703 (72) Guàrdia, E.; Pinzón, R.; Casulleras, J.; Orozco, M.; Luque, F.J. *Mol. Sim.*
704 **2001**, *26*, 287–306.
- 705 (73) Nikitin, A.M.; Lyubartsev, A.P. *J. Comput. Chem.* **2007**, *28*, 2020–2026.
- 706 (74) Hloucha, M.; Deiters, U.K. *Mol. Phys.* **1997**, *90*, 593–597.
- 707 (75) Alper, H.E.; Abu-Awwad, F.; Politzer, P. *J. Phys. Chem. B* **1999**, *103*,
708 9738–9742.
- 709 (76) Sorescu, D.C.; Rice, B.M.; Thompson, D.L. *J. Phys. Chem. A* **2001**, *105*,
710 9336–9346.
- 711 (77) Price, M.L.P.; Ostrovsky, D.; Jorgensen, W.L. *J. Comput. Chem.* **2001**,
712 *22*, 1340–1352.
- 713 (78) Wick, C.D.; Stubbs, J.M.; Rai, N.; Siepmann, J.I. *J. Phys. Chem. B* **2005**,
714 *109*, 18974–18982.
- 715 (79) Vrabec, J.; Kettler, M.; Hasse, H. *Chem. Phys. Lett.* **2002**, *356*, 431–436.

- 716 (80) Andersen, H.C. *J. Chem. Phys.* **1980**, *72*, 2384–2393.
- 717 (81) Widom, B. *J. Chem. Phys.* **1963**, *39*, 2808–2812.
- 718 (82) Nezbeda, I.; Kolafa, J. *Mol. Sim.* **1991**, *5*, 391–403.
- 719 (83) Lustig, R. *Mol. Phys.* **1988**, *65*, 175–179.
- 720 (84) Flyvbjerg, H.; Petersen, H.G. *J. Chem. Phys.* **1989**, *91*, 461–466.

TABLE 1: Parameters of the new molecular models. Lennard-Jones interaction sites are denoted by the modeled atoms (in boldface) with an additional bonding partner if necessary. Electrostatic interaction sites are denoted by dipole or quadrupole, respectively. Coordinates are given with respect to the center of mass in a principal axes system. Orientations of the electrostatic sites are defined in standard Euler angles, where φ is the azimuthal angle with respect to the $x - z$ plane and θ is the inclination angle with respect to the z axis.

Interaction Site	x Å	y Å	z Å	σ Å	ε/k_B K	θ deg	φ deg	μ D	Q B
Iso-butane									
CH	0	0	0.8179	3.360	51.00	—	—	—	—
CH₃(1)	1.7302	0	-0.1893	3.607	120.15	—	—	—	—
CH₃(2)	-0.8651	1.4984	-0.1893	3.607	120.15	—	—	—	—
CH₃(3)	-0.8651	-1.4984	-0.1893	3.607	120.15	—	—	—	—
Dipole	0	0	0	—	—	0	0	0.1347	—
Quadrupole	0	0	0	—	—	0	0	—	0.7236
Cyclohexane									
CH₂(1)	0.0210	-0.3118	1.8052	3.497	87.39	—	—	—	—
CH₂(2)	1.5318	0.2989	0.8863	3.497	87.39	—	—	—	—
CH₂(3)	-1.5528	0.2983	0.9986	3.497	87.39	—	—	—	—
CH₂(4)	1.5318	-0.2989	-0.8863	3.497	87.39	—	—	—	—
CH₂(5)	-1.5528	-0.2983	-0.9986	3.497	87.39	—	—	—	—
CH₂(6)	0.0210	0.3118	-1.8052	3.497	87.39	—	—	—	—
Quadrupole	0	0	0	—	—	90	90	—	0.8179
Formaldehyde									
O	0	0	0.6721	3.010	112.61	—	—	—	—
CH₂	0	0	-0.7682	3.422	77.42	—	—	—	—
Dipole	0	0	0.0480	—	—	180	0	2.6668	—

continued on next page

continued from previous page

Interaction Site	x Å	y Å	z Å	σ Å	ε/k_B K	θ deg	φ deg	μ D	Q B
Dimethyl Ether									
O	0	0	0.6427	2.727	89.57	—	—	—	—
CH₃(1)	1.4041	0	-0.3086	3.607	120.15	—	—	—	—
CH₃(2)	-1.4041	0	-0.3086	3.607	120.15	—	—	—	—
Dipole	0	0	0	—	—	180	0	1.7040	—
Sulfur Dioxide									
S	0	0	0.3757	3.312	139.23	—	—	—	—
O(1)	1.2790	0	-0.3653	3.106	43.18	—	—	—	—
O(2)	-1.2790	0	-0.3653	3.106	43.18	—	—	—	—
Dipole	0	0	0	—	—	0	0	1.9980	—
Quadrupole	0	0	0	—	—	90	0	—	-5.3340
Dimethyl Sulfide									
S	0	0	0.2819	3.398	207.57	—	—	—	—
CH₃(1)	1.1583	0	-0.3868	3.607	120.15	—	—	—	—
CH₃(2)	-1.1583	0	-0.3868	3.607	120.15	—	—	—	—
Dipole	0	0	0	—	—	90	180	2.3610	—
Quadrupole	0	0	0	—	—	90	0	—	3.0740
Quadrupole	0	0	0	—	—	0	0	—	2.7600
Thiophene									
S	0	0	0.7359	4.292	95.65	—	—	—	—
CH(1)-S	1.2513	0	0.2067	3.590	48.49	—	—	—	—
CH(2)-S	-1.2513	0	0.2067	3.590	48.49	—	—	—	—
CH(3)-CH	0.7734	0	-1.2643	3.590	48.49	—	—	—	—
CH(4)-CH	-0.7734	0	-1.2643	3.590	48.49	—	—	—	—
Dipole	0	0	0	—	—	180	0	1.8120	—
Quadrupole	0	0	0	—	—	90	0	—	6.5389

continued on next page

continued from previous page

Interaction Site	x Å	y Å	z Å	σ Å	ε/k_B K	θ deg	φ deg	μ D	Q B
Hydrogen Cyanide									
N	0	0	0.6380	3.233	39.69	—	—	—	—
CH	0	0	-0.9671	3.445	102.44	—	—	—	—
Dipole	0	0	0.0589	—	—	180	0	3.4084	—
Quadrupole	0	0	0.0589	—	—	0	0	—	2.1800
Acetonitrile									
N	0	0	1.1507	3.368	53.00	—	—	—	—
C	0	0	0.0507	2.810	10.64	—	—	—	—
CH₃	0	0	-1.2868	3.835	163.04	—	—	—	—
Dipole	0	0	0	—	—	180	0	4.1186	—
Quadrupole	0	0	0	—	—	0	0	—	-3.1373
Nitromethane									
N	0	0	0.2199	3.321	34.90	—	—	—	—
O(1)	1.1045	0	0.7858	3.060	45.17	—	—	—	—
O(2)	-1.1045	0	0.7858	3.060	45.17	—	—	—	—
CH₃	0	0	-1.5135	3.501	158.79	—	—	—	—
Dipole	0	0	0.2535	—	—	180	0	3.9901	—
Quadrupole	0	0	0.2535	—	—	90	0	—	-4.7903

TABLE 2: Critical properties: present simulation results compared to recommended experimental data. The numbers in parentheses indicate the experimental uncertainty in the last digits.

	T_c^{sim}	T_c^{exp}	ρ_c^{sim}	ρ_c^{exp}	p_c^{sim}	p_c^{exp}	Ref.
	K	K	mol/l	mol/l	MPa	MPa	
Iso-butane	407	407.8(5)	3.87	3.86(5)	3.65	3.64(5)	[38]
Cyclohexane	556	553.8(2)	3.26	3.25(2)	4.23	4.08(3)	[38]
Formaldehyde	406	408	8.38	8.70	5.95	6.59	[39]
Dimethyl Ether	403	400.2(1)	5.99	5.95(2)	5.69	5.34(5)	[40]
Sulfur Dioxide	425	430.7(1)	8.15	8.2 (8)	7.22	7.9 (4)	[41]
Dimethyl Sulfide	511	503 (1)	4.95	4.91(8)	5.46	5.53(10)	[42]
Hydrogen Cyanide	448	457 (1)	7.89	7.4 (1)	4.69	5.4 (1)	[43]
Acetonitrile	540	545.5(1)	6.04	5.8 (1)	4.95	4.85(3)	[43]
Nitromethane	587	588 (1)	5.87	5.8 (0)	5.98	6.3 (1)	[44]

List of Figures

722	1	Geometry of the united-atom sites: (a) The methine (CH) site is	
723		located at 0.4 of the carbon-hydrogen distance, (b) the methylene	
724		(CH ₂) site is located at the geometric mean, and (c) the methyl	
725		(CH ₃) site is located at the geometric mean.	35
726	2	Saturated densities. Present simulation data: ● iso-butane, □ cy-	
727		clohexane, ○ dimethyl ether. — correlations of experimental data	
728		[35], + critical points derived from simulation, ▼ experimental	
729		critical points.	36
730	3	Vapor pressure. Present simulation data: ● iso-butane, ■ cyclo-	
731		hexane, ○ dimethyl ether. — correlations of experimental data	
732		[35], + critical points derived from simulation, ▼ experimental	
733		critical points.	37
734	4	Enthalpy of vaporization. Present simulation data: ● iso-butane,	
735		■ cyclohexane, ○ dimethyl ether. — correlations of experimental	
736		data [35].	38
737	5	Relative deviations of vapor-liquid equilibrium properties between	
738		simulation data and correlations of experimental data [35] ($\delta z =$	
739		$(z_{\text{sim}} - z_{\text{exp}})/z_{\text{exp}}$) for iso-butane: ● present model, ○ Martin and	
740		Siepmann [49], □ Nath and de Pablo [48]. Top: vapor pressure,	
741		center: saturated liquid density, bottom: enthalpy of vaporization.	39
742	6	Relative deviations of vapor-liquid equilibrium properties between	
743		simulation data and correlations of experimental data [35] ($\delta z =$	
744		$(z_{\text{sim}} - z_{\text{exp}})/z_{\text{exp}}$) for cyclohexane: ● present model, ○ Bourasseau	
745		et al. [50]. Top: vapor pressure, center: saturated liquid density,	
746		bottom: enthalpy of vaporization.	40
747	7	Saturated densities. Present simulation data: ● formaldehyde,	
748		■ hydrogen cyanide, ◆ acetonitrile, ○ nitromethane. — corre-	
749		lations of experimental data [35], + critical points derived from	
750		simulation, ▼ experimental critical points.	41

751	8	Enthalpy of vaporization. Present simulation data: ● formalde-	
752		hyde, ■ hydrogen cyanide, ◆ acetonitrile, ○ nitromethane. —	
753		correlations of experimental data [35].	42
754	9	Relative deviations of vapor-liquid equilibrium properties between	
755		simulation data and correlations of experimental data [35] ($\delta z =$	
756		$(z_{\text{sim}} - z_{\text{exp}})/z_{\text{exp}}$) for present models: ● formaldehyde, ■ hy-	
757		drogen cyanide, ▲ sulfur dioxide. Top: vapor pressure, center:	
758		saturated liquid density, bottom: enthalpy of vaporization.	43
759	10	Relative deviations of vapor-liquid equilibrium properties between	
760		simulation data and correlations of experimental data [35] ($\delta z =$	
761		$(z_{\text{sim}} - z_{\text{exp}})/z_{\text{exp}}$) for dimethyl ether: ● present model, ○ Stubbs	
762		et al. [60], □ Ketko and Potoff [61]. Top: vapor pressure, center:	
763		saturated liquid density, bottom: enthalpy of vaporization.	44
764	11	Saturated densities. Present simulation data: ● sulfur dioxide,	
765		■ dimethyl sulfide, ○ thiophene. — correlations of experimental	
766		data [35], + critical points derived from simulation, ▼ experimen-	
767		tal critical points, cf. Table 2.	45
768	12	Vapor pressure. Present simulation data: ● sulfur dioxide, ■ dimethyl	
769		sulfide, ○ thiophene. — correlations of experimental data [35],	
770		+ critical points derived from simulation, ▼ experimental critical	
771		points.	46
772	13	Enthalpy of vaporization. Present simulation data: ● sulfur diox-	
773		ide, ■ dimethyl sulfide, ○ thiophene. — correlations of experi-	
774		mental data [35].	47
775	14	Relative deviations of vapor-liquid equilibrium properties between	
776		simulation data and correlations of experimental data [35] ($\delta z =$	
777		$(z_{\text{sim}} - z_{\text{exp}})/z_{\text{exp}}$) for dimethyl sulfide: ● present model, ○ Lubna	
778		et al. [68]. Top: vapor pressure, center: saturated liquid density,	
779		bottom: enthalpy of vaporization.	48

780	15	Relative deviations of vapor-liquid equilibrium properties between	
781		simulation data and correlations of experimental data [35] ($\delta z =$	
782		$(z_{\text{sim}} - z_{\text{exp}})/z_{\text{exp}}$) for thiophene: ● present model, ○ Lubna et	
783		al. [68], □ Juárez-Guerra et al. [69], △ Pérez-Pellitero et al. [70].	
784		Top: vapor pressure, center: saturated liquid density, bottom:	
785		enthalpy of vaporization.	49
786	16	Relative deviations of vapor-liquid equilibrium properties between	
787		simulation data and correlations of experimental data [35] ($\delta z =$	
788		$(z_{\text{sim}} - z_{\text{exp}})/z_{\text{exp}}$) for acetonitrile: ● present model, ○ Wick et	
789		al. [78], □ Jorgensen and Briggs [71, 78]. Top: vapor pressure,	
790		center: saturated liquid density, bottom: enthalpy of vaporization.	50
791	17	Relative deviations of vapor-liquid equilibrium properties between	
792		simulation data and correlations of experimental data [35] ($\delta z =$	
793		$(z_{\text{sim}} - z_{\text{exp}})/z_{\text{exp}}$) for nitromethane: ● present model, ○ Wick	
794		et al. [78], □ Price et al. [77]. Top: vapor pressure, center:	
795		saturated liquid density, bottom: enthalpy of vaporization.	51

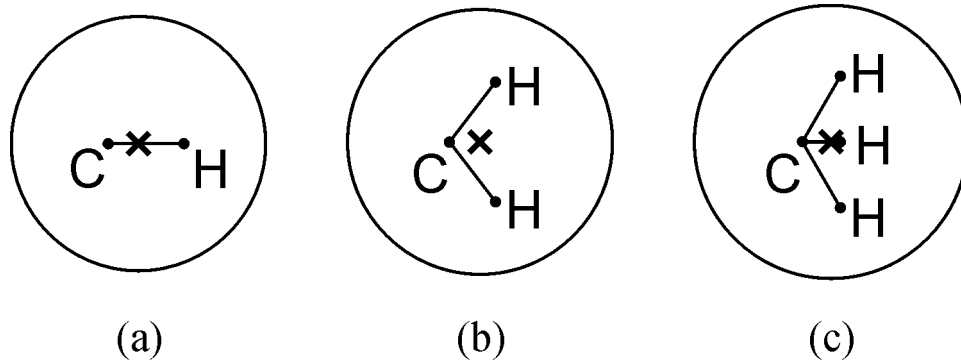


Figure 1. Eckl et al.

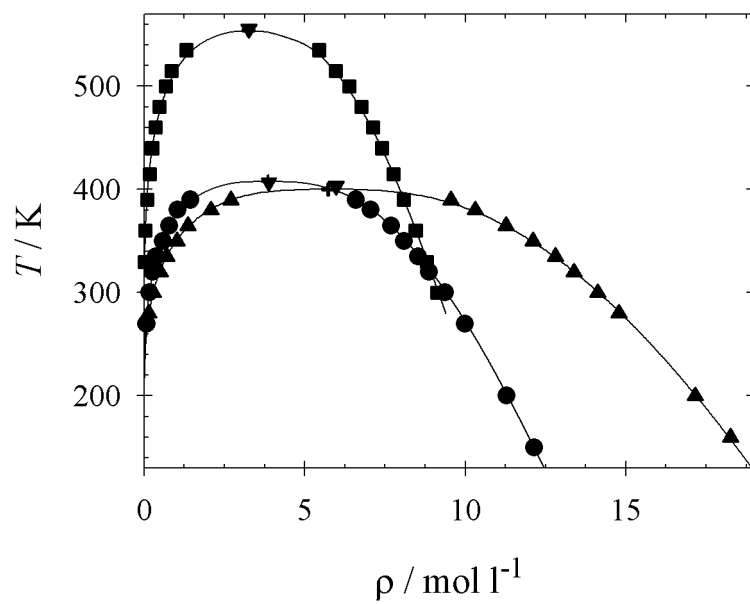


Figure 2. Eckl et al.

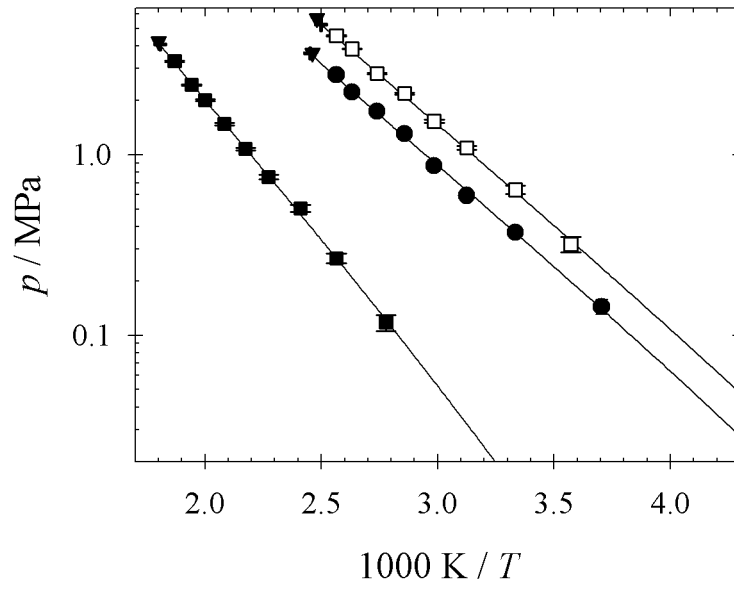


Figure 3. Eckl et al.

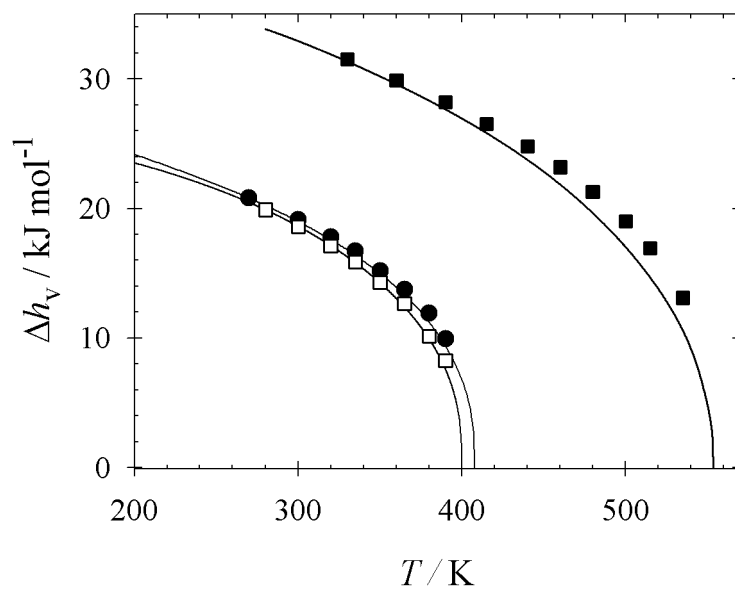


Figure 4. Eckl et al.

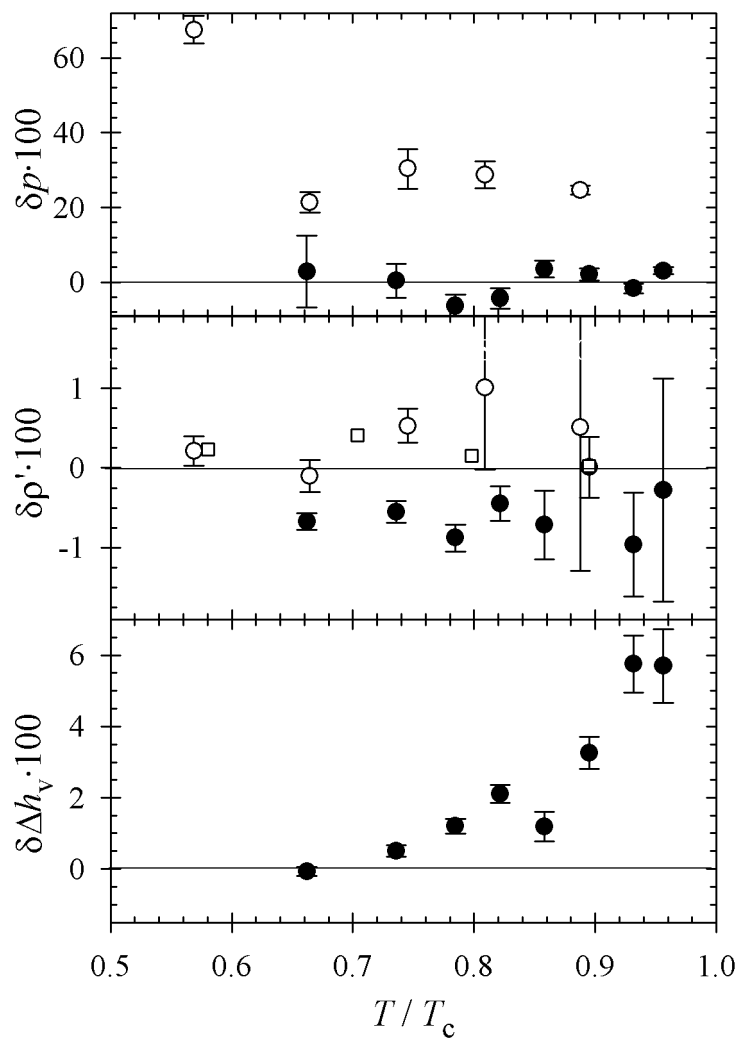


Figure 5. Eckl et al.

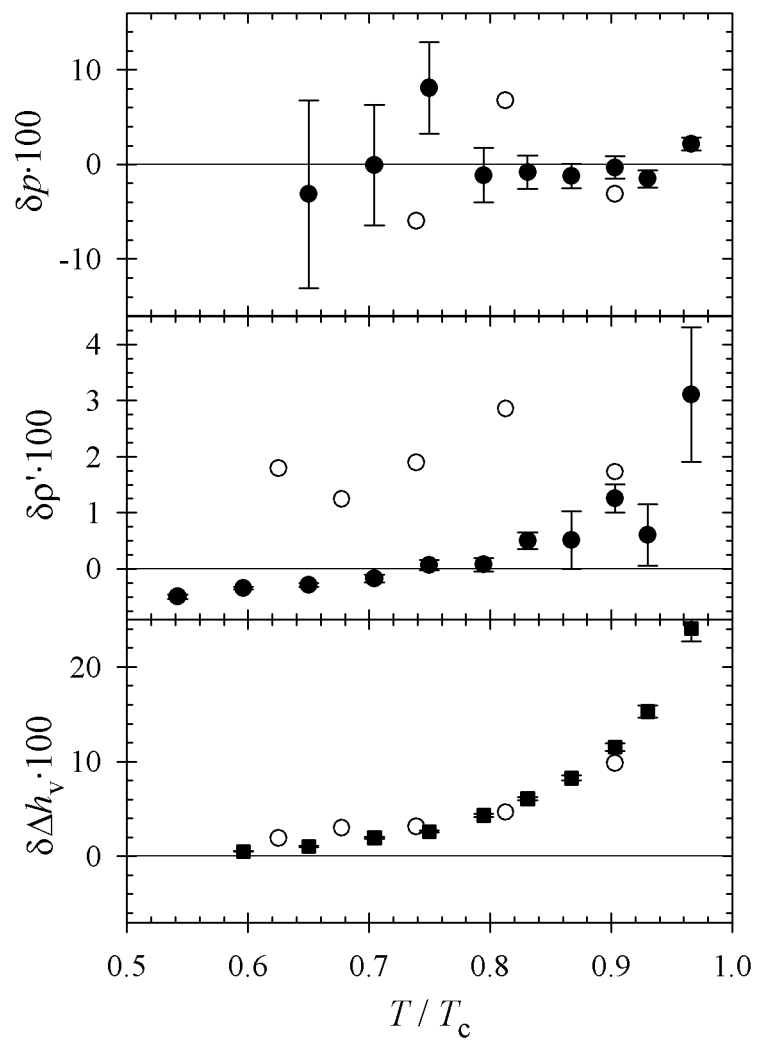


Figure 6. Eckl et al.

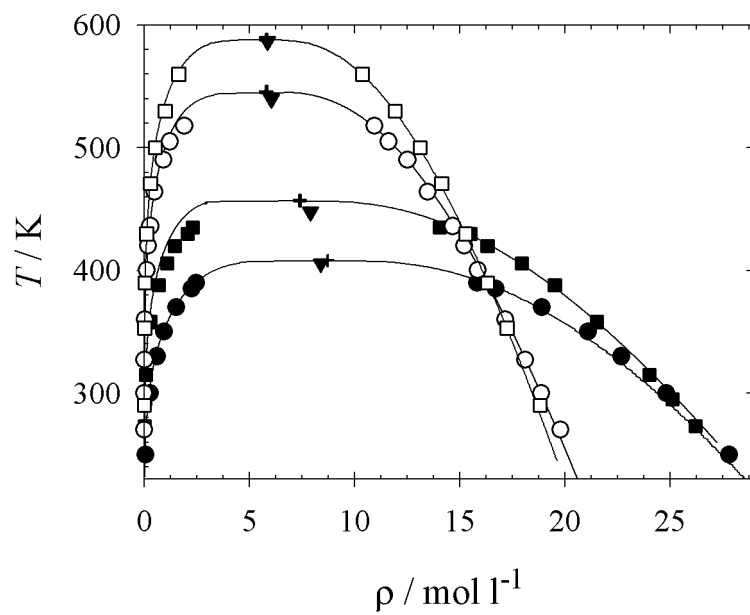


Figure 7. Eckl et al.

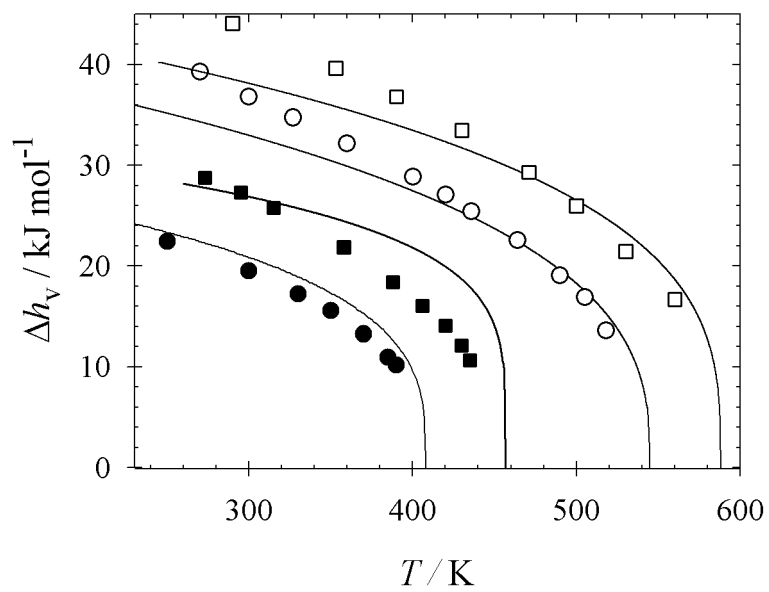


Figure 8. Eckl et al.

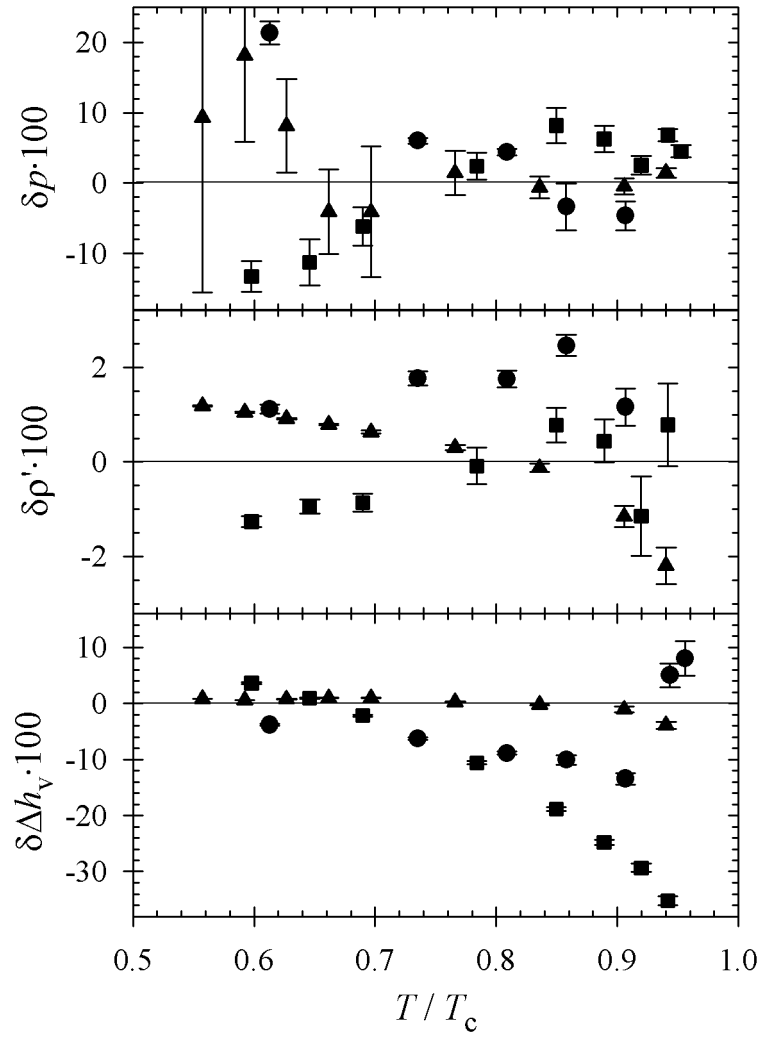


Figure 9. Eckl et al.

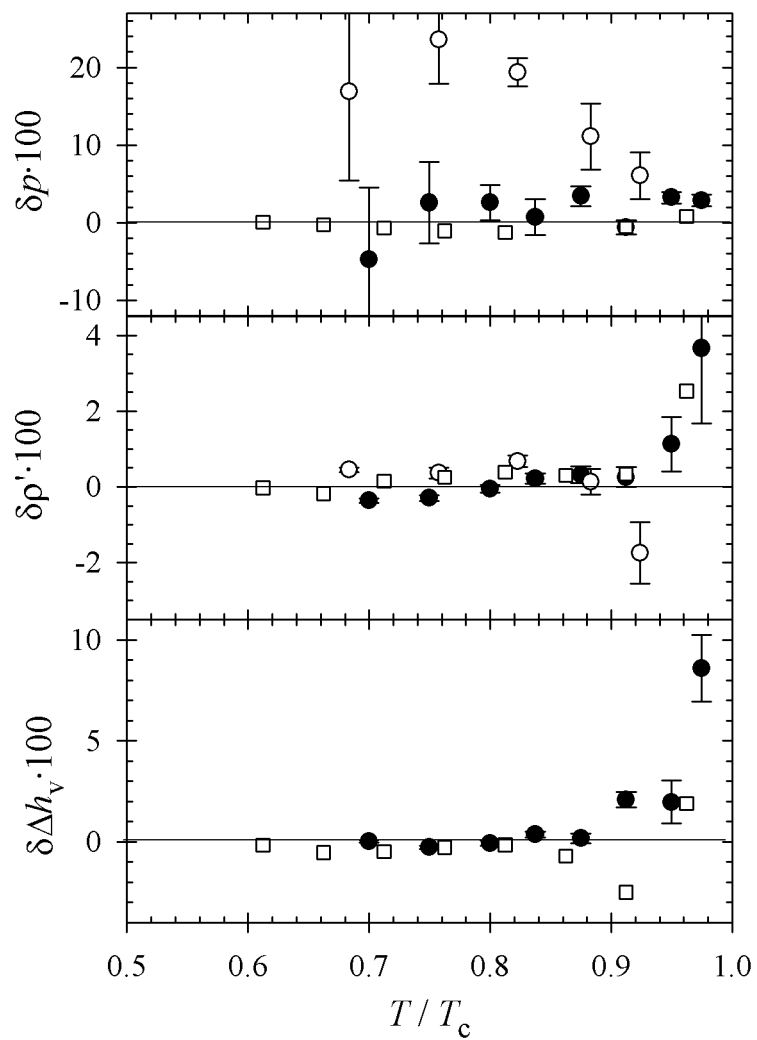


Figure 10. Eckl et al.

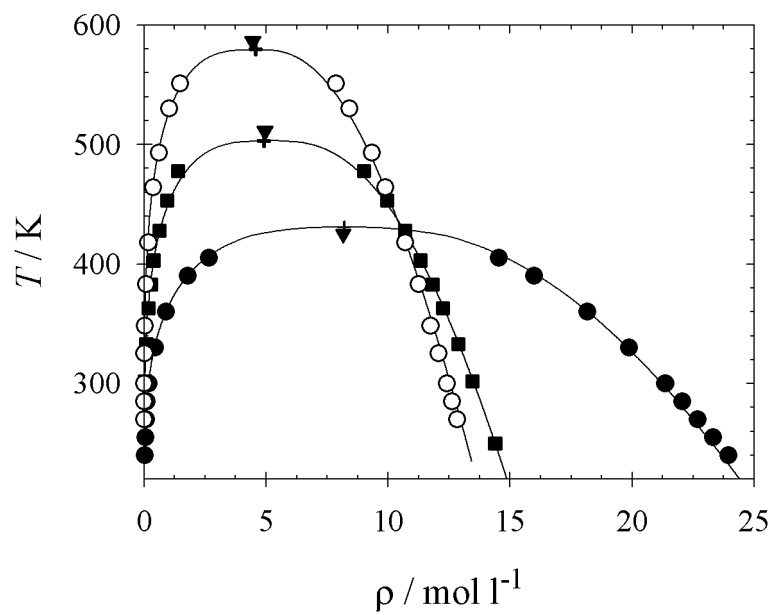


Figure 11. Eckl et al.

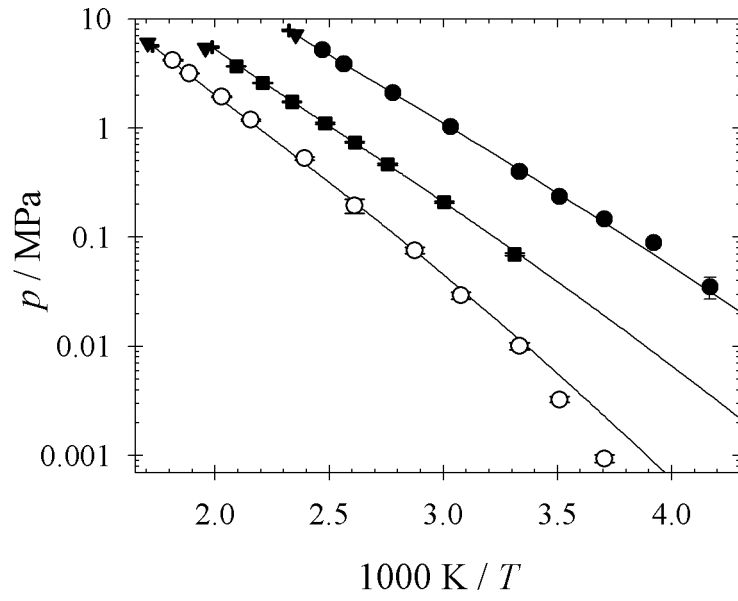


Figure 12. Eckl et al.

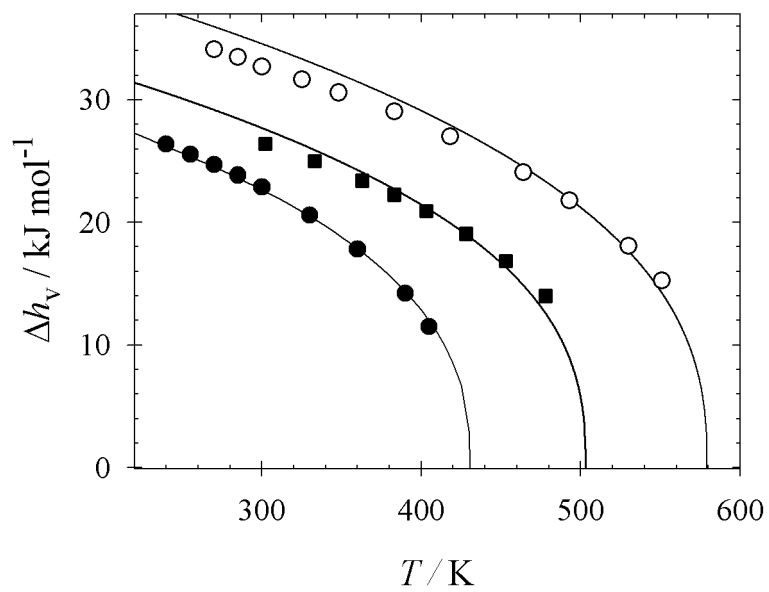


Figure 13. Eckl et al.

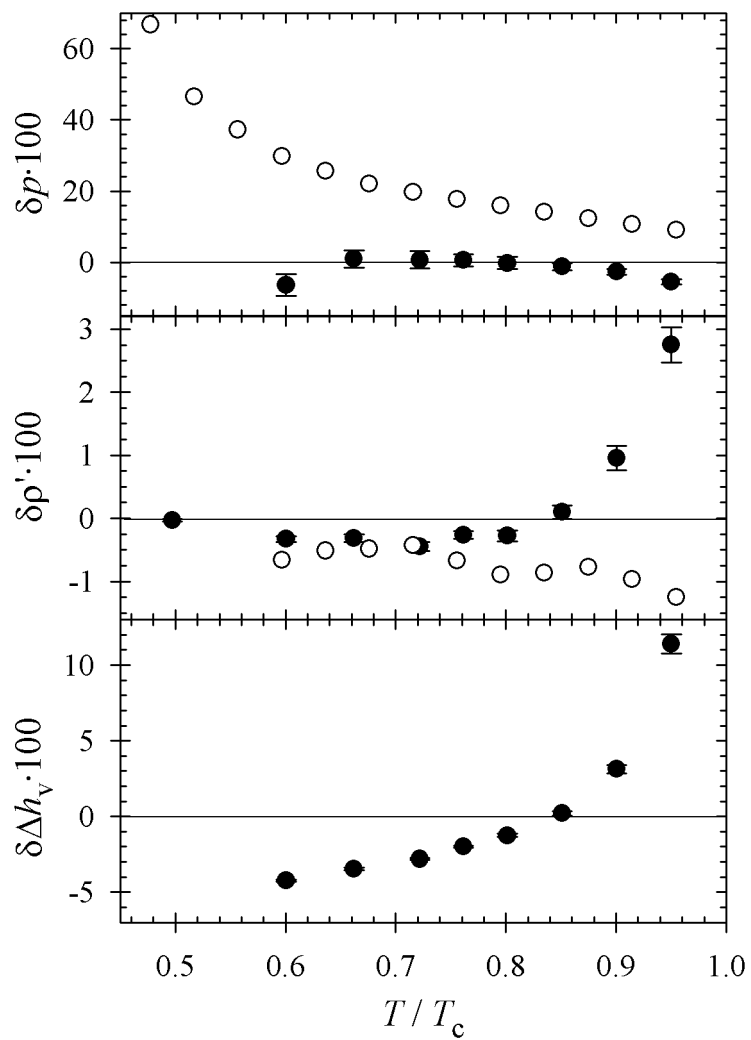


Figure 14. Eckl et al.

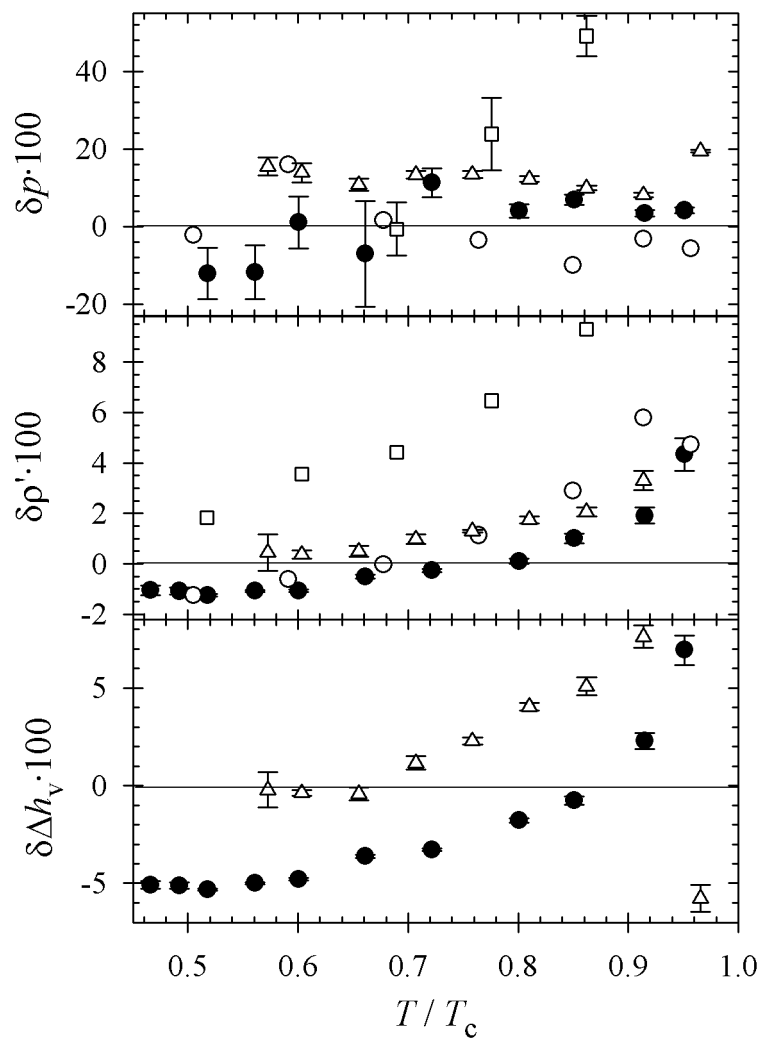


Figure 15. Eckl et al.

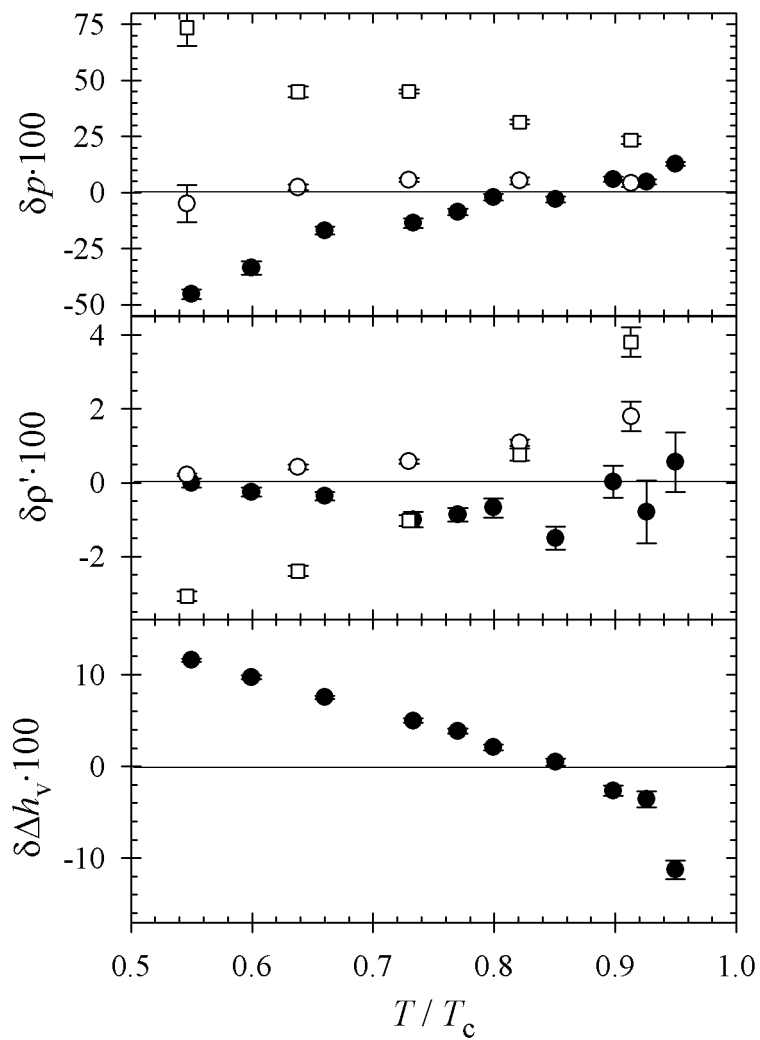


Figure 16. Eckl et al.

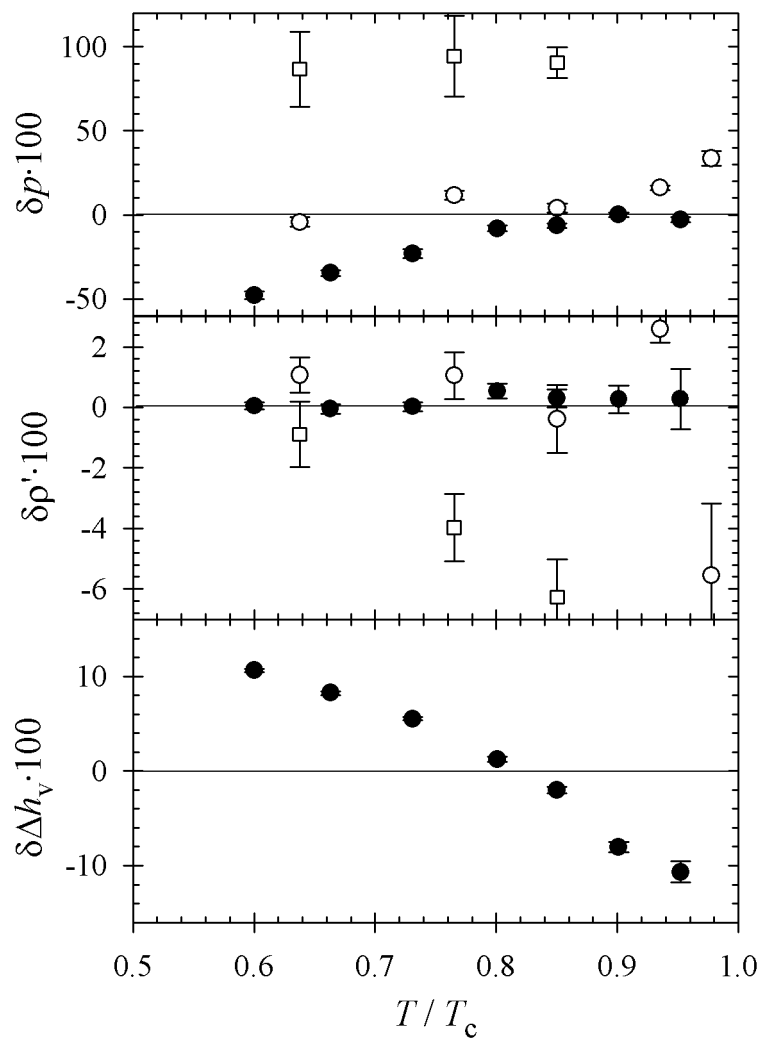


Figure 17. Eckl et al.

796 **Supplementary Material**

TABLE 3: Vapor-liquid equilibria of the modeled substances: present simulation results compared to experimental data [35] for vapor pressure, saturated densities and heat of vaporization. The number in parentheses indicates the statistical uncertainty in the last digit.

T K	p_{σ}^{sim} MPa	p_{σ}^{exp} MPa	ρ'_{sim} mol/l	ρ'_{exp} mol/l	ρ''_{sim} mol/l	$\Delta h_{\text{v}}^{\text{sim}}$ kJ/mol	$\Delta h_{\text{v}}^{\text{exp}}$ kJ/mol
Iso-butane							
150			12.15(1)	12.149			
200			11.28(1)	11.325			
270	0.14(1)	0.140	9.98(1)	10.050	0.067(6)	20.80(3)	20.811
300	0.37(2)	0.370	9.37(1)	9.420	0.164(7)	19.10(3)	19.006
320	0.59(2)	0.633	8.88(2)	8.955	0.254(8)	17.80(4)	17.591
335	0.87(2)	0.906	8.54(2)	8.575	0.37 (1)	16.72(4)	16.375
350	1.30(3)	1.258	8.10(3)	8.159	0.58 (1)	15.16(6)	14.980
365	1.74(3)	1.701	7.69(3)	7.688	0.79 (1)	13.76(6)	13.325
380	2.21(3)	2.252	7.05(5)	7.113	1.03 (2)	11.89(9)	11.240
390	2.77(3)	2.689	6.59(9)	6.609	1.44 (2)	9.9 (1)	9.408
Cyclohexane							
300			9.13(0)	9.174			
330	0.02(1)	0.046	8.80(0)	8.831	0.013(3)	31.49(1)	31.339
360	0.12(1)	0.121	8.45(0)	8.476	0.041(4)	29.89(1)	29.589
390	0.27(2)	0.267	8.09(1)	8.101	0.088(5)	28.19(2)	27.646
415	0.51(2)	0.467	7.77(1)	7.767	0.165(7)	26.50(3)	25.828
440	0.75(2)	0.763	7.41(1)	7.404	0.240(7)	24.78(3)	23.758
460	1.08(2)	1.085	7.12(1)	7.083	0.343(6)	23.18(4)	21.853
480	1.48(2)	1.496	6.76(3)	6.723	0.478(7)	21.27(5)	19.647
500	2.01(2)	2.012	6.38(2)	6.305	0.68 (1)	18.99(7)	17.027
515	2.44(2)	2.478	5.97(3)	5.935	0.85 (1)	16.92(9)	14.675
535	3.29(2)	3.223	5.44(6)	5.280	1.31 (2)	13.1 (1)	10.566
Formaldehyde							
250	0.103(1)	0.085	27.81(3)	27.50	0.053(1)	22.41(4)	23.30
300	0.582(2)	0.549	24.83(4)	24.40	0.273(3)	19.49(5)	20.80
330	1.327(6)	1.271	22.69(4)	22.30	0.617(7)	17.22(5)	18.90
350	1.99 (7)	2.058	21.11(5)	20.60	0.95 (7)	15.6 (2)	17.30
370	3.03 (7)	3.180	18.92(7)	18.70	1.53 (8)	13.2 (2)	15.30
385	4.12 (7)	4.298	16.7 (1)	16.90	2.24 (9)	10.9 (2)	13.20
390	4.49 (9)	4.732	15.8 (2)	16.20	2.5 (1)	10.2 (3)	12.20

continued on next page

continued from previous page

T K	p_{σ}^{sim} MPa	p_{σ}^{exp} MPa	ρ'_{sim} mol/l	ρ'_{exp} mol/l	ρ''_{sim} mol/l	$\Delta h_{\text{v}}^{\text{sim}}$ kJ/mol	$\Delta h_{\text{v}}^{\text{exp}}$ kJ/mol
Dimethyl Ether							
160			18.25(1)	18.209			
200			17.17(1)	17.189			
280	0.32(3)	0.335	14.79(1)	14.844	0.15(1)	19.90(1)	19.896
300	0.64(3)	0.623	14.11(1)	14.156	0.29(1)	18.57(2)	18.623
320	1.09(2)	1.065	13.39(1)	13.401	0.49(1)	17.11(2)	17.124
335	1.53(4)	1.523	12.80(2)	12.772	0.70(1)	15.86(2)	15.806
350	2.18(3)	2.110	12.11(3)	12.067	1.02(1)	14.29(4)	14.262
365	2.83(3)	2.843	11.27(3)	11.242	1.36(2)	12.65(5)	12.391
380	3.86(3)	3.742	10.31(7)	10.196	2.09(3)	10.1 (1)	9.950
390	4.57(3)	4.444	9.6 (2)	9.215	2.69(4)	8.3 (1)	7.625
Sulfur Dioxide							
240	0.04(1)	0.032	23.945(3)	23.664	0.018(4)	26.40(1)	26.197
255	0.09(1)	0.069	23.327(3)	23.085	0.043(4)	25.53(1)	25.375
270	0.15(1)	0.136	22.694(3)	22.488	0.069(4)	24.71(1)	24.521
285	0.24(1)	0.247	22.043(4)	21.869	0.106(6)	23.85(1)	23.623
300	0.40(4)	0.417	21.357(8)	21.222	0.17 (1)	22.88(1)	22.667
330	1.03(3)	1.013	19.88 (1)	19.816	0.44 (1)	20.57(1)	20.511
360	2.09(3)	2.098	18.17 (2)	18.190	0.90 (2)	17.83(3)	17.867
390	3.85(4)	3.873	15.98 (4)	16.166	1.80 (3)	14.20(7)	14.354
405	5.17(3)	5.095	14.53 (6)	14.855	2.66 (3)	11.50(7)	11.967
Dimethyl Sulfide							
250			14.385(3)	14.390			
302	0.070(2)	0.0747	13.448(7)	13.492	0.028(1)	26.43(1)	27.607
333	0.210(5)	0.2082	12.865(8)	12.906	0.080(2)	25.02(2)	25.917
363	0.47 (1)	0.4647	12.233(8)	12.288	0.169(4)	23.41(2)	24.086
383	0.74 (1)	0.7352	11.809(7)	11.841	0.261(5)	22.27(2)	22.726
403	1.11 (2)	1.1092	11.32 (1)	11.355	0.387(7)	20.95(2)	21.216
428	1.74 (2)	1.7584	10.68 (1)	10.673	0.609(7)	19.07(3)	19.034
453	2.59 (2)	2.6616	9.95 (2)	9.857	0.93 (1)	16.85(5)	16.336
478	3.68 (3)	3.8885	9.01 (2)	8.770	1.39 (2)	14.01(8)	12.580
Thiophene							
270	0.0009(1)	0.0023	12.83 (2)	12.967	0.0004(1)	34.13(7)	35.956
285	0.0033(2)	0.0054	12.62 (2)	12.763	0.0014(1)	33.46(6)	35.270
300	0.0101(8)	0.0115	12.398(6)	12.555	0.0041(3)	32.72(2)	34.562
325	0.029 (2)	0.0333	12.068(6)	12.199	0.0110(9)	31.67(2)	33.329
348	0.076 (5)	0.0753	11.732(6)	11.859	0.027 (2)	30.59(2)	32.127
383	0.19 (3)	0.2089	11.257(8)	11.315	0.063 (9)	29.06(2)	30.148
418	0.53 (2)	0.4755	10.699(6)	10.728	0.166 (5)	27.02(2)	27.939
464	1.18 (2)	1.1389	9.88 (1)	9.866	0.359 (6)	24.09(3)	24.532
493	1.94 (2)	1.8132	9.33 (2)	9.238	0.599 (8)	21.76(5)	21.928
530	3.17 (2)	3.0679	8.42 (3)	8.264	1.03 (1)	18.06(7)	17.653
551	4.20 (3)	4.0312	7.86 (5)	7.530	1.46 (2)	15.2 (1)	14.240

continued on next page

continued from previous page

T K	p_{σ}^{sim} MPa	p_{σ}^{exp} MPa	ρ'_{sim} mol/l	ρ'_{exp} mol/l	ρ''_{sim} mol/l	$\Delta h_{\text{v}}^{\text{sim}}$ kJ/mol	$\Delta h_{\text{v}}^{\text{exp}}$ kJ/mol
Hydrogen Cyanide							
273	0.030(1)	0.0350	26.21(3)	26.548	0.0141(4)	28.78(4)	27.778
295	0.078(3)	0.0877	25.11(4)	25.354	0.035 (1)	27.30(4)	27.060
315	0.169(5)	0.1798	24.01(5)	24.217	0.074 (2)	25.76(5)	26.336
358	0.66 (1)	0.6400	21.52(8)	21.536	0.292 (6)	21.86(7)	24.451
388	1.43 (3)	1.3255	19.52(7)	19.367	0.69 (1)	18.41(8)	22.697
406	2.09 (4)	1.9655	17.9 (8)	17.859	1.08 (2)	16.0 (1)	21.323
420	2.69 (3)	2.6261	16.3 (1)	16.504	1.44 (3)	14.1 (1)	19.953
430	3.43 (3)	3.2072	15.5 (1)	15.373	2.05 (3)	12.1 (1)	18.690
435	3.70 (3)	3.5377	14.0 (3)	14.726	2.31 (3)	10.7 (2)	17.909
Acetonitrile							
270	0.0015(1)	0.0029	19.71(1)	19.636	0.0007(1)	38.87(8)	34.302
300	0.0074(3)	0.0132	18.90(2)	18.871	0.0032(1)	36.78(7)	32.952
327	0.029 (1)	0.0396	18.20(3)	18.151	0.0112(6)	34.88(7)	31.641
360	0.088 (3)	0.119	17.25(2)	17.223	0.033 (1)	32.42(6)	29.886
400	0.294 (5)	0.352	16.05(2)	16.003	0.109 (2)	29.09(6)	27.459
420	0.51 (1)	0.558	15.47(4)	15.341	0.190 (4)	27.27(8)	26.078
436	0.76 (3)	0.782	14.78(1)	14.777	0.289 (9)	25.31(5)	24.866
450	1.00 (4)	1.032	14.25(2)	14.253	0.38 (1)	23.98(5)	23.705
464	1.27 (9)	1.341	13.65(3)	13.693	0.48 (3)	22.58(5)	22.427
490	2.08 (4)	2.101	12.42(3)	12.515	0.85 (2)	19.20(9)	19.603
505	2.69 (3)	2.673	11.52(5)	11.707	1.18 (2)	16.7 (1)	17.549
510	2.73 (5)	2.889	11.06(6)	11.405	1.16 (2)	16.5 (1)	16.753
518	3.14 (4)	3.263	10.37(7)	10.871	1.37 (2)	15.0 (1)	15.308
Nitromethane							
290	0.001(1)	0.0031	18.82(2)	18.669	0.0003(1)	44.05(4)	38.511
353	0.026(1)	0.0503	17.25(2)	17.239	0.0092(4)	39.62(5)	35.812
390	0.105(3)	0.1602	16.32(3)	16.331	0.035 (1)	36.78(7)	33.983
430	0.33 (1)	0.4354	15.27(2)	15.270	0.107 (3)	33.47(5)	31.716
471	0.92 (2)	1.0033	14.13(3)	14.058	0.301 (6)	29.29(8)	28.931
500	1.56 (2)	1.6696	13.12(4)	13.083	0.525 (8)	25.98(9)	26.518
530	2.70 (4)	2.6942	11.93(5)	11.899	0.99 (2)	21.5 (1)	23.347
560	4.09 (6)	4.2110	10.4 (1)	10.345	1.64 (3)	16.7 (2)	18.696

